International Journal of Non–Linear Mechanics 159 (2024) 104619

Contents lists available at ScienceDirect

International Journal of Non-Linear Mechanics

journal homepage: www.elsevier.com/locate/nlm

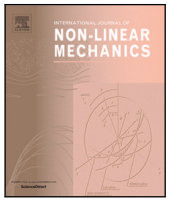

A unified buckling formulation for linear and nonlinear analysis of laminated plates using penalty based C^0 FEM-HSDT model

Surendra Verma [a,*,1], Abha Gupta [b,2], Babu Ranjan Thakur [c,2], Donatus Oguamanam [a,3], B.N. Singh [d,4]

[a] Department of Mechanical, Industrial, and Mechatronics Engineering, Toronto Metropolitan University, Toronto, Ontario M5B 2K3, Canada
[b] School of Mechanical Engineering, VIT Bhopal University, Bhopal, Madhya Pradesh 466114, India
[c] Department of Aerospace Engineering, Punjab Engineering College (DU), Chandigarh 160012, India
[d] Department of Aerospace Engineering, IIT Kharagpur, Kharagpur, West Bengal 721302, India

ARTICLE INFO

Keywords:
Buckling analysis
Green–Lagrange nonlinearity
Higher-order shear deformation theory
Finite element method

ABSTRACT

In this paper, the effect of pre-buckling boundary conditions and the type of nonlinearity for stress stiffening used in different linear and nonlinear buckling approaches is studied for laminated composite plates. The study is conducted using a C^0 finite element (FE) plate model, employing a unified C^1 higher-order shear deformation theory (HSDT). The set of governing equations is derived using the principle of virtual displacement and solved using the tangent-based arc-length method in conjunction with a simple branch switching technique. The performance of the present C^0 FE model is assessed through a validation exercise and comparison with results obtained via the use of ANSYS and, for linear analysis, Navier solution, as well as solutions available in the literature. The influence of the different in-plane loads, boundary conditions, side-to-thickness ratio, fiber orientation, types of imperfection and penalty stiffness matrix are also examined. The results show that the same boundary conditions must be utilized in both pre-buckling and linear eigenvalue analyses for accurate and realistic predictions of critical buckling loads, as confirmed from the nonlinear buckling analyses. Furthermore, the critical buckling loads obtained using Green–Lagrange nonlinearity are observed to be more conservative than those obtained using von Kármán nonlinearity. The nonlinear buckling approach is a generalized approach while the nonlinear eigenvalue approach has a limited range of application.

1. Introduction

Laminated composite structures are finding increasing use across many industries. The primary reasons for their use include their high specific stiffness and strength, the ability to tailor their properties via optimized stacking sequence and ply thickness [1], improved manufacturing methods and understanding of their mechanical properties. Generally, laminated composite plate structures are widely utilized and are often subjected to in-plane mechanical loads that could lead to instability [2]. Further, these plate structures, irrespective of their thicknesses, are susceptible to transverse shear deformation due to their low transverse shear moduli relative to their in-plane Young's moduli. Thus, the importance of considering the effect of transverse shear deformation in the design and stability analysis of composite plates cannot be overemphasized [3].

The design and stability analysis of laminated composite or multilayered plates are commonly based on three approaches: equivalent plate theories [3], layerwise or zigzag [4], and Carrera's unified formulation (CUF) [5]. Equivalent plate theories are predominantly used to determine the response of composite plates in the presence of various loading scenarios because the resulting formulation has a tendency to produce results of acceptable accuracy at low computational cost and are easily implementable [6]. The first and simplest equivalent plate theory is the classical laminated plate theory (CLPT) which assumes transverse normality, constant transverse deformation, and the absence of transverse shear deformation [7]. This theory is suitable for thin

* Corresponding author.
E-mail addresses: suri@torontomu.ca (S. Verma), abhagupta@vitbhopal.ac.in (A. Gupta), baburanjanthakur@pec.edu.in (B.R. Thakur), doguaman@torontomu.ca (D. Oguamanam), bnsingh@aero.iitkgp.ac.in (B.N. Singh).
[1] Post-Doctoral Research Fellow.
[2] Assistant Professor.
[3] Associate Professor.
[4] Professor.

https://doi.org/10.1016/j.ijnonlinmec.2023.104619
Received 19 September 2023; Received in revised form 8 December 2023; Accepted 11 December 2023
Available online 18 December 2023

plates and not for thick plates where it overpredicts stiffness and, therefore, underestimate deflection, and overestimate natural frequencies and buckling loads. The first-order shear deformation theory (FSDT), also called the Reissner–Mindlin plate theory, relaxes the transverse normality condition and assumes a constant transverse shear. This theory is suitable for moderately thick plates but requires a shear correction factor and does not satisfy the theory of elasticity equations at the surface of the plates because it yields non-zero traction at the top and bottom surfaces.

The Reddy's third-order shear deformation theory (TSDT) is the simplest type of the so called higher-order shear deformation theories (HSDTs). It predicts a parabolic distribution of transverse shear strain with traction-free boundary conditions at the top and bottom surfaces and yields accurate structural analysis (bending, vibration, and buckling analysis) even for thick plates [7]. In addition to HSDTs, there are higher-order shear and normal deformation theories (HSNDTs) that have more than five field variables and capture thickness stretching. Notwithstanding, a five-field-variable HSDT is employed in this paper because of its simpler formulation, lower computational cost, and acceptable accuracy when compared to the HSNDTs [6]. A generalized C^1 HSDT model is employed in this study so that TSDT, FSDT, CLPT, and a wide range of non-polynomial shear deformation theories (NPSDTs) can be deduced by the choice of an appropriate boundary conditions and transverse shear function, $f(z)$ (see Section 2).

The set of governing equations corresponding to equivalent plate theories is solved via the use of various analytical and approximate solution methodologies [3] to simulate the response of a composite structures. The finite element method is the most popular numerical approximate solution methodology due to its wide range of applicability and established mathematical foundation. The finite element method supports both C^0 and C^1 continuity formulation, but the former is more widely used because it is easier to implement (often as Lagrange interpolations). There are few open source finite element packages that support C^1 continuous Hermite approximations [8]. However, in the C^0 finite element formulation C^1 requirement of HSDT is satisfied using either penalty approach or Lagrange multiplier approach. The penalty approach is employed in this study because it requires smaller computation cost and provides ease in the implementation.

Thin laminated composite plates are extensively used in industry, particularly aerospace and maritime. These plates are susceptible to buckling failure when subjected to compression loads, and, very often, this failure precedes others. Hence, buckling failure is a strength failure [7]. It is plausible to conclude, therefore, that any reliable design of these structures must incorporate an estimate of their elastic stability and the effect of the geometric stiffness matrix (also called stress stiffening). The literature is replete with many linear [4,9–15] and nonlinear buckling studies [10,11,16–18] to predict the buckling strength of composite plates that are exposed to in-plane mechanical loads. Dennis and Palazotto [9] highlight the importance of using in-plane Green–Lagrange strain in formulations for accurate predictions of buckling strength of plates. Shufrin and Eisenberger [19] observe a decrease of 7.5% in the buckling load of rectangular plates when nonlinear curvature terms are included in the expression of strain. Similarly, Ruocco and Minutolo [12,13] conclude that models that employ the von Kármán nonlinearity overestimate the critical load compared to those that use nonlinear in-plane strain.

In linear buckling analysis a primarily eigenvalue problem is solved to obtain the critical buckling load or load multiplier. While unrealistic and impracticable, uniform stress distribution is assumed for the stress stiffening effect in the aforementioned studies. The distribution of stress depends upon various factors, including the distribution of external in-plane loads, boundary conditions, interaction with the adjoining parts, and the presence of discontinuities such as holes. Hence, many studies [20–24] that employ a two-stage analysis have been reported. The first stage comprises a pre-buckling analysis using pre-buckling boundary conditions, and it is followed by a second stage where a linear eigenvalue buckling analysis is performed using buckling boundary conditions. In these studies, stress stiffening effect is captured via the use of von Kármán nonlinearity only, and a uniform stress distribution is obtained due to the consideration of pre-buckling boundary conditions. Refs. [25,26] use buckling boundary conditions as the pre-buckling conditions. Patel and Sheikh [25] used Green–Lagrange nonlinearity to capture stress stiffening effect. They do not compare the effect of using either pre-buckling or buckling boundary conditions, especially their effect on buckling strength. Nima and Ganesan [26] report the effect of using different pre-buckling boundary conditions on buckling strength. A validation study of the Ritz method against the commercial finite element software ANSYS results is reported. A comprehensive study of the effect of in-plane boundary condition on the elastic buckling behavior of perforated and nonperforated plates is reported by Prajapati et al. [27]. It is observed that plates loaded under a constant strain exhibit higher buckling load than those loaded under constant stress. Hence, it is conservative to design composite structures under constant stress loading, and this informs the approach employed in the present study.

Plates do not usually lose their entire stability at the initial bifurcation load, but follow a secondary path, called post-buckling path, before terminating at the failure criteria. For such problems, a nonlinear analysis is essential to obtain the limit load, equilibrium path, and other details that a linear buckling analysis cannot provide. There are numerous nonlinear buckling analysis based investigations [17,28–35] to predict the pre-buckling, buckling, and post-buckling characteristics of composite plates under in-plane loading using FSDT [17,28], TSDT [32,33], HSDT [29], UTSDT [31], HSNDT [30], and CUF [34–36]. While most of the these studies uses von Kármán nonlinearity, Bhimaraddi [33] observes a difference of 2.5% between Green–Lagrange and von Kármán based results for thick plates. The study by Dash and Singh [30] on the post-buckling characteristics of composite plates via nonlinear eigenvalue approach consider only Green–Lagrange nonlinearity. Similarly, Wu et al. [34] and Carrera et al. [36] employed only Green–Lagrange nonlinearity to investigate the post-buckling behavior of isotropic slender structures and anisotropic flat panels, respectively. Particularly, Pagani et al. [35] and Xu et al. [5] highlight the importance of a full nonlinear model (Green–Lagrange nonlinearity) over a von Kármán model in the post-buckling region. It is plausible to infer from the literature that there is less clarity on the consequence of using either von Kármán or Green–Lagrange nonlinearities.

Generally, not all problems can be grouped under the category of bifurcation buckling. For example, problems of plates with imperfection, bending-stretching coupling, or partial edge loading are not eigenvalue problems [16,17]. In this context, Le-Manh and Lee [16] investigated the nonlinear buckling response of laminated composite plate under in-plane mechanical load with and without imperfection. A NURBS-based isogeometric approach that uses FSDT with small rotation Green–Lagrange and von Kármán nonlinearities is employed. Recently, Tran and Kim [17] investigated the effect of initial imperfection on buckling and post-buckling behavior of multilayered plates by employing FSDT and von Kármán nonlinearity via isogeometric approach. These studies do not examine the applicability of HSDT (particularly NPSDT) in nonlinear buckling analysis. The post-buckling equilibrium path of multilayered composite plates is often traced by nonlinear eigenvalue or buckling approach, but there is no comprehensive comparative study to examine the reliability of the nonlinear eigenvalue approach.

The buckling behavior of the composite plates is extensively studied using linear buckling approaches compared to (geometrically) nonlinear approaches where von Kármán nonlinearity is often employed. While great strides have been made in the development of numerous new NPSDT, there is a paucity of studies in linear and nonlinear buckling analysis using NPSDT with full geometric nonlinearity [3]. Further, the role of pre-buckling boundary conditions, effect of penalty stiffness matrix, and the reliability of nonlinear eigenvalue and nonlinear buckling approaches have not been adequately studied. The same

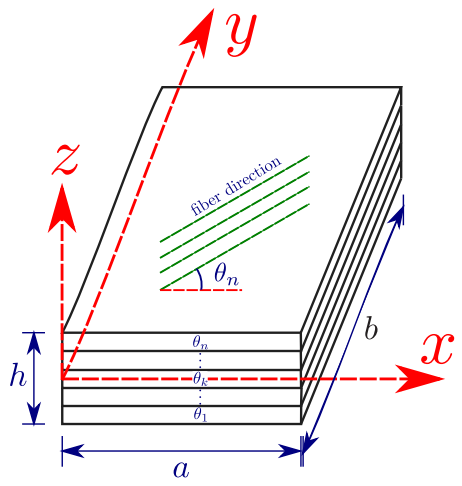

Fig. 1. Schematic diagram of multilayered composite plate with xyz coordinate system.

can be said about the effect of different in-plane mechanical loads, which should reflect or capture the loading conditions a composite panel may experience during its operational and service life.

The investigation reported in this paper is a comprehensive examination of the buckling analysis of laminated composite plates due to in-plane mechanical loads using a unified formulation of a penalty based C^0 FEM-HSDT model. For modeling purposes, a generalized C^1 HSDT model is used so that the solution for each NPSDT or PSDT can be readily obtained by the mere substitution of the particular transverse shear function (see Section 2.1) with appropriate boundary conditions. A nine-node Lagrange finite element is employed and the buckling response is obtained using the arc-length method in conjunction with a simple branch-switching technique [37,38]. The advantage of using Green–Lagrange nonlinearity over von Kármán nonlinearity is established via validation and comparative studies. The role of pre-buckling boundary conditions, penalty parameter, and solution methodology (or approach) on accurate and reliable buckling analysis is discussed. The results reveal that the nonlinear buckling approach is the most reliable. Further, the same boundary conditions must be used in the two-stage linear buckling analysis.

The rest of the paper is organized as follows: Section 2 describes the mathematical formulation; in Section 3, the accuracy of the present C^0 FEM-HSDT model is established by comparing the results with ANSYS results and with results in the literature; Section 4 outlines conclusions that are inferred from the study, and the use of the nonlinear buckling approach with Green–Lagrange nonlinearity for buckling analysis via TSDT is suggested.

2. Mathematical formulation

Consider a multilayered rectangular composite plate that is composed of n elastic orthotropic layers with stacking sequence $(\theta_1/\theta_2/\ldots/\theta_n)$, length a, width b, and uniform thickness h. A Cartesian coordinate system xyz, where xy plane coincides with the midplane of the plate, is defined as shown in Fig. 1.

2.1. Higher-order shear deformation theory

The kinematics of the multilayered composite plate is defined via an equivalent higher-order shear deformation theory. To readily permit comparisons between different non-polynomial shear deformation theories (including TSDT), the field variables are given as

$$\begin{aligned} u(x,y,z) &= u_0(x,y) - z\frac{\partial w_0}{\partial x} + f(z)\,\theta_x(x,y) \\ v(x,y,z) &= v_0(x,y) - z\frac{\partial w_0}{\partial y} + f(z)\,\theta_y(x,y) \\ w(x,y,z) &= w_0(x,y) \end{aligned} \tag{1}$$

where u, v, w are displacements in x, y, and z directions, respectively; u_0, v_0, and w_0 are the corresponding midplane displacements; θ_x and θ_y are the shear deformation of the normal to the midplane about y-axis and x-axis, respectively; and $f(z)$ is a transverse shear function. A polynomial shear deformation theory (PSDT) is defined when $f(z)$ is a polynomial function else it is a non-polynomial shear deformation theory (NPSDT). In general, $f(z)$ is selected such that zero transverse shear deformation at top and bottom surfaces of the plate is satisfied. The different plate theories used in present study are discussed in Section 3.

Most finite element method approaches use Lagrange basis functions, with C^0 continuity, unlike Hermite basis function, with C^1 continuity, because of the difficulty of their implementation due to the increased continuity requirement [8]. Artificial field variables can be introduced to reduce the continuity of the field variables to C^0 and then permits the re-write of Eq. (1) for C^1 HSDT as

$$\begin{aligned} u(x,y,z) &= u_0(x,y) + z\phi_x(x,y) + f(z)\,\theta_x(x,y) \\ v(x,y,z) &= v_0(x,y) + z\phi_y(x,y) + f(z)\,\theta_y(x,y) \\ w(x,y,z) &= w_0(x,y) \end{aligned} \tag{2}$$

where $\phi_x = -\frac{\partial w_0}{\partial x}$ and $\phi_y = -\frac{\partial w_0}{\partial y}$. Hence the C^1 HSDT model has seven field variables $\boldsymbol{u} = \{u_0\ v_0\ w_0\ \phi_x\ \phi_y\ \theta_x\ \theta_y\}^T$, where ^{T} denotes *transpose* of a matrix.

2.2. Strain–displacement relation

The Green–Lagrange nonlinearity strain vector $\boldsymbol{\varepsilon}$ at a point may be expressed as

$$\boldsymbol{\varepsilon} = \boldsymbol{\varepsilon}_l + \frac{1}{2}\boldsymbol{\varepsilon}_{nl} + \boldsymbol{\varepsilon}^* \tag{3}$$

where

$$\boldsymbol{\varepsilon}_l = \begin{Bmatrix} \frac{\partial u}{\partial x} \\ \frac{\partial v}{\partial y} \\ \frac{\partial u}{\partial y} + \frac{\partial v}{\partial x} \\ \frac{\partial v}{\partial z} + \frac{\partial w}{\partial y} \\ \frac{\partial u}{\partial z} + \frac{\partial w}{\partial x} \end{Bmatrix}; \boldsymbol{\varepsilon}_{nl} = \begin{Bmatrix} \left(\frac{\partial u}{\partial x}\right)^2 + \left(\frac{\partial v}{\partial x}\right)^2 + \left(\frac{\partial w}{\partial x}\right)^2 \\ \left(\frac{\partial u}{\partial y}\right)^2 + \left(\frac{\partial v}{\partial y}\right)^2 + \left(\frac{\partial w}{\partial y}\right)^2 \\ 2\left(\frac{\partial u}{\partial x}\frac{\partial u}{\partial y} + \frac{\partial v}{\partial x}\frac{\partial v}{\partial y} + \frac{\partial w}{\partial x}\frac{\partial w}{\partial y}\right) \\ 2\left(\frac{\partial u}{\partial y}\frac{\partial u}{\partial z} + \frac{\partial v}{\partial y}\frac{\partial v}{\partial z} + \frac{\partial w}{\partial y}\frac{\partial w}{\partial z}\right) \\ 2\left(\frac{\partial u}{\partial x}\frac{\partial u}{\partial z} + \frac{\partial v}{\partial x}\frac{\partial v}{\partial z} + \frac{\partial w}{\partial x}\frac{\partial w}{\partial z}\right) \end{Bmatrix};$$

$$\boldsymbol{\varepsilon}^* = \begin{Bmatrix} \frac{\partial w}{\partial x}\frac{\partial w^*}{\partial x} \\ \frac{\partial w}{\partial y}\frac{\partial w^*}{\partial y} \\ \frac{\partial w}{\partial x}\frac{\partial w^*}{\partial y} + \frac{\partial w}{\partial y}\frac{\partial w^*}{\partial x} \\ 0 \\ 0 \end{Bmatrix}$$

and, $\boldsymbol{\varepsilon}_l$, $\frac{1}{2}\boldsymbol{\varepsilon}_{nl}$, and $\boldsymbol{\varepsilon}^*$ denote the linear, nonlinear, and imperfection component of the strain vector $\boldsymbol{\varepsilon}$, respectively. The imperfection (or initial deflection in the transverse direction) can be of a different shape and nature (i.e., local or global [15,17,39]), and it is denoted by the symbol w^*. Unless stated otherwise, the default profile of the imperfection employed in this study is limited to a sinusoidal shape such that $w^* = hw_0^* sin(\pi x/a)\,sin(\pi y/b)$ with relative imperfection amplitude w_0^*. This is equivalent to the first buckling mode in linear

buckling analysis, and displacements are measured from the imperfect configuration which is taken as the reference configuration.

By using the expression of the modified displacement relation (Eq. (2)), linear strain vector $\boldsymbol{\varepsilon}_l$, nonlinear strain vector $\boldsymbol{\varepsilon}_{nl}$, and strain due to imperfection $\boldsymbol{\varepsilon}^*$ can be separated into in-plane strain vector and transverse strain vector as:

$$\boldsymbol{\varepsilon}_l = \begin{Bmatrix} \boldsymbol{\varepsilon}_{lb} \\ \boldsymbol{\varepsilon}_{ls} \end{Bmatrix} = \begin{Bmatrix} \boldsymbol{Z}_{lb}\hat{\boldsymbol{\varepsilon}}_{lb} \\ \boldsymbol{Z}_{ls}\hat{\boldsymbol{\varepsilon}}_{ls} \end{Bmatrix} = \boldsymbol{Z}_l\hat{\boldsymbol{\varepsilon}}_l\,;$$
$$\boldsymbol{\varepsilon}_{nl} = \begin{Bmatrix} \boldsymbol{\varepsilon}_{nlb} \\ \boldsymbol{\varepsilon}_{nls} \end{Bmatrix} = \begin{Bmatrix} \boldsymbol{Z}_{nlb}\hat{\boldsymbol{\varepsilon}}_{nlb} \\ \boldsymbol{Z}_{nls}\hat{\boldsymbol{\varepsilon}}_{nls} \end{Bmatrix} = \boldsymbol{Z}_{nl}\hat{\boldsymbol{\varepsilon}}_{nl}\,;\ \boldsymbol{\varepsilon}^* = \begin{Bmatrix} \boldsymbol{Z}_{lb}\hat{\boldsymbol{\varepsilon}}_b^* \\ 0 \end{Bmatrix} = \boldsymbol{Z}_l\hat{\boldsymbol{\varepsilon}}^* \tag{4}$$

The components of the these matrices are presented in Ref. [8].

2.3. Constitutive relation

The constitutive relation for an arbitrary kth orthotropic layer of multilayered plate with zero transverse normal stress condition may be expressed as:

$$\boldsymbol{\sigma} = \bar{\boldsymbol{Q}}^{(k)}\boldsymbol{\varepsilon} = \left[T_{\text{trans}}^{(k)}\right]\boldsymbol{Q}^{(k)}\left[T_{\text{trans}}^{(k)}\right]^T\boldsymbol{\varepsilon} \tag{5}$$

where $\boldsymbol{\sigma}$, $\boldsymbol{\varepsilon}$, and $\bar{\boldsymbol{Q}}$ are stress, strain, and material matrix, respectively; $\boldsymbol{Q}^{(k)}$ denotes the material matrix in the local coordinate system. Further, stress-resultants are defined by taking the integral of stress terms across the thickness. The explicit relation and details of the transformation matrix $\left(\left[T_{\text{trans}}^{(k)}\right]\right)$, material matrix $\left(\bar{\boldsymbol{Q}}^{(k)}\right)$, and stress-resultants are presented in Ref. [8].

2.4. Variational principle

For admissible virtual displacement $\delta\{u, v, w\}$, the principle of virtual work for the given system may be written as:

$$\int_V \left[\delta\{\boldsymbol{\varepsilon}\}^T\{\boldsymbol{\sigma}\} + \delta\left(\frac{\partial w_0}{\partial x} + \phi_x\right)^T\gamma\left(\frac{\partial w_0}{\partial x} + \phi_x\right) + \delta\left(\frac{\partial w_0}{\partial y} + \phi_y\right)^T\gamma\left(\frac{\partial w_0}{\partial y} + \phi_y\right)\right]dV = \int_s\left(\delta u_0 n_x + \delta v_0 n_y\right)P_i\,ds \tag{6}$$

where all kinematics and stress variables are measured with respect to the imperfect configuration or reference configuration (i.e., total Lagrangian approach). The first term in the left-hand side of the equation represents the virtual strain energy and it may be written in an expanded form as

$$\delta U = \int_V (\delta\boldsymbol{\varepsilon})^T\boldsymbol{\sigma}\,dz\,d\Omega = \int_V\left(\delta\boldsymbol{\varepsilon}_l + \delta\boldsymbol{\varepsilon}_{nl} + \delta\boldsymbol{\varepsilon}^*\right)\bar{Q}^{(k)} \times\left(\boldsymbol{\varepsilon}_l + \frac{1}{2}\boldsymbol{\varepsilon}_{nl} + \boldsymbol{\varepsilon}^*\right)dz\,d\Omega \tag{7a}$$

$$= \left[\left\{\left[\left(\delta\hat{\boldsymbol{\varepsilon}}_l\right)^T + \left(\delta\hat{\boldsymbol{\varepsilon}}^*\right)^T\right]\boldsymbol{Z}_l^T + \left(\delta\hat{\boldsymbol{\varepsilon}}_{nl}\right)^T\boldsymbol{Z}_{nl}^T\right\}\bar{Q}^{(k)} \times\left\{\boldsymbol{Z}_l\left[\hat{\boldsymbol{\varepsilon}}_l + \hat{\boldsymbol{\varepsilon}}^*\right] + \frac{1}{2}\boldsymbol{Z}_{nl}\hat{\boldsymbol{\varepsilon}}_{nl}\right\}\right]dz\,d\Omega \tag{7b}$$

Still on the left-hand side of the Eq. (6), the second and third terms together represent virtual strain energy, δU_γ, due to artificial constraints [40]:

$$\delta U_\gamma = \int_V\gamma\left[\delta\left(\frac{\partial w_0}{\partial x} + \phi_x\right)^T\left(\frac{\partial w_0}{\partial x} + \phi_x\right) + \delta\left(\frac{\partial w_0}{\partial y} + \phi_y\right)^T\left(\frac{\partial w_0}{\partial y} + \phi_y\right)\right]dz\,dA \tag{8}$$

where γ is the penalty parameter. The right-hand side terms of Eq. (6) represent the virtual work done by the in-plane mechanical load and it is expressed as

$$\delta W_{ext} = \int_s\left(\delta u_0 n_x + \delta v_0 n_y\right)P_i|_{z=0}\,ds \tag{9}$$

where $P_i(x, y)|_{z=0}$ denotes the in-plane mechanical line load acting normal to the reference edge line with n_x and n_y denoting the direction cosine of (in-plane) normal to cross-sectional area. The present study is limited to non-follower mechanical loads.

2.5. Total Lagrangian finite element formulation

The plate is discretized using nine-noded isoparametric Lagrange elements as shown in Fig. 2.

Following the definition of shape functions from geometric description, the displacement field variables (Eq. (2)) can be interpolated at an arbitrary point (x, y) as:

$$\boldsymbol{u} = \sum_{i=1}^{9} I_7 N_i\boldsymbol{q}_i \tag{10}$$

where I_7 denotes a 7×7 identity matrix, and $\boldsymbol{q}_i$ represents the vector of seven nodal displacement field variable or degree of freedom, i.e., $\boldsymbol{q}_i=\{u_{0i}, v_{0i}, w_{0i}, \phi_{xi}, \phi_{yi}, \theta_{xi}, \theta_{yi}\}^T$ corresponding to ith node with $N_i(\xi, \eta)$ shape function.

The uncoupled characteristics of an orthotropic material is exploited to decompose the strain energy into bending and transverse shear components to simplify the finite element code implementation. To this end, Eq. (10) is substituted into Eq. (4) and the resulting generalized strain vector $\hat{\boldsymbol{\varepsilon}}$ can be rewritten in terms of elemental strain–displacement matrix $\boldsymbol{B}$ and elemental displacement vector $\boldsymbol{q}$ as:

$$\hat{\boldsymbol{\varepsilon}}_{lj} = \sum_{i=1}^{9}\boldsymbol{B}_{ji}^L\boldsymbol{q}_i = \boldsymbol{B}_j^L\boldsymbol{q};\ \ \hat{\boldsymbol{\varepsilon}}_b^* = \sum_{i=1}^{9}\boldsymbol{B}_{bi}^*\boldsymbol{q}_i = \boldsymbol{B}_b^*\boldsymbol{q};$$
$$\hat{\boldsymbol{\varepsilon}}_{nlj} = \sum_{i=1}^{9}\boldsymbol{A}_j\boldsymbol{G}_{ij}^{NL}\boldsymbol{q}_j = \sum_{i=1}^{9}\boldsymbol{B}_{ji}^{NL}\boldsymbol{q}_i = \boldsymbol{B}_j^{NL}\boldsymbol{q}$$
$$\boldsymbol{q} = \left\{\boldsymbol{q}_1^T\ \ \boldsymbol{q}_2^T\ \ \cdots\ \ \boldsymbol{q}_8^T\ \ \boldsymbol{q}_9^T\right\}^T \tag{11}$$

in which $j = b$ for bending (ε_b) and $j = s$ for transverse shear (ε_s).

The explicit expressions of $\boldsymbol{B}_j^L$, $\boldsymbol{B}_b^*$ and $\boldsymbol{G}_j^{NL}$ contain terms which require first derivative of the Lagrange basis function $\left(\frac{\partial N_i}{\partial x}\right)$ which is related to the corresponding derivative in the natural coordinates $\left(\frac{\partial N_i}{\partial\xi}, \frac{\partial N_i}{\partial\eta}\right)$ via the Jacobian [8].The explicit expressions of strain–displacement matrices $(\boldsymbol{B})$ can be found in Refs. [8,41].

2.6. System of equations

By using Eq. (11) in Eq. (7), and Eq. (10) in Eq. (9), and applying variational method concept to Eq. (6), the set of governing equations for the geometrically nonlinear static analysis of the composite plate under mechanical loads may be written as

$$\left(\boldsymbol{K} + \gamma\boldsymbol{K}_\gamma\right)\boldsymbol{q} = \boldsymbol{F}_{P_i} \tag{12}$$

where the stiffness

$$\boldsymbol{K} = \int_V\Big(\left(\boldsymbol{B}^L + \boldsymbol{B}^*\right)^T\boldsymbol{Z}_l^T\bar{\boldsymbol{Q}}\boldsymbol{Z}_l\left(\boldsymbol{B}^L + \boldsymbol{B}^*\right) + \frac{1}{2}\left(\boldsymbol{B}^L + \boldsymbol{B}^*\right)^T\boldsymbol{Z}_l^T\bar{\boldsymbol{Q}}\boldsymbol{Z}_{nl}\boldsymbol{B}^{NL} + \left(\boldsymbol{B}^{NL}\right)^T\boldsymbol{Z}_{nl}^T\bar{\boldsymbol{Q}}\boldsymbol{Z}_l\left(\boldsymbol{B}^L + \boldsymbol{B}^*\right) + \frac{1}{2}\left(\boldsymbol{B}^{NL}\right)^T\boldsymbol{Z}_{nl}^T\bar{\boldsymbol{Q}}\boldsymbol{Z}_{nl}\boldsymbol{B}^{NL}\Big)dz\,dA \tag{13}$$

the stiffness matrix due to artificial constraints

$$\boldsymbol{K}_\gamma = \int_V\left[\boldsymbol{B}_\gamma\right]^T\left[\boldsymbol{B}_\gamma\right]dz\,dA \tag{14}$$

and, the mechanical force vector due to in-plane mechanical loads

$$\boldsymbol{F}_{P_i} = \int_s\{\mathscr{U}\}^T P_i(x, y)\,ds$$

with

$$\{\mathscr{U}\}^T\{\boldsymbol{q}\} = \sum_{i=1}^{9}\left\{\mathscr{U}_i\right\}^T\boldsymbol{q}_i;\ \ \left\{\mathscr{U}_i\right\}^T = \left\{n_x N_i\ \ \ n_y N_i\ \ \ 0\ \ \ 0\ \ \ 0\ \ \ 0\ \ \ 0\right\}$$

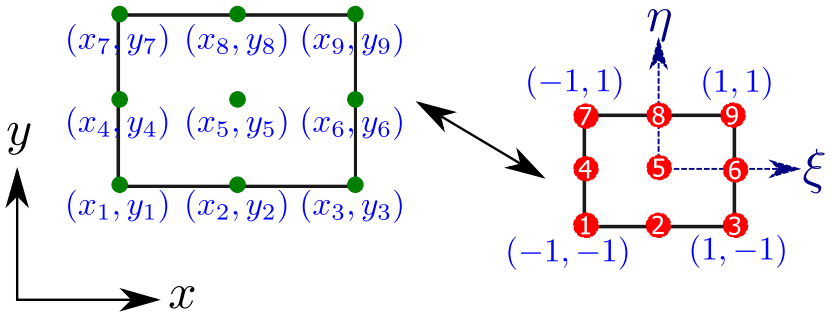

Fig. 2. Nine noded isoparametric element.

The explicit relation of penalty stiffness matrix $\boldsymbol{K}_\gamma$ is provided in Ref. [8].

2.7. Solution procedure

A solution procedure for Eq. (12) is presented in this section. The nonlinear global system of equations that results after assembly of the element equations and the imposition of suitable boundary conditions are solved iteratively. The solution path is traced via the use of the arc-length iterative method [42] and the tangent stiffness matrix $\boldsymbol{K}_T$ is given as

$$\boldsymbol{K}_T = \boldsymbol{K}_L + \boldsymbol{K}_{NL} + \gamma \boldsymbol{K}_\gamma + \boldsymbol{K}_\sigma$$

where $\boldsymbol{K}_\sigma$ is the geometric stiffness matrix and the sum of $\boldsymbol{K}_L$ and $\boldsymbol{K}_{NL}$ is given as

$$\boldsymbol{K}_L + \boldsymbol{K}_{NL} = \int_V \left[\left\{ \left(\boldsymbol{B}^L + \boldsymbol{B}^*\right)^T \boldsymbol{Z}_l^T + \left(\boldsymbol{B}^{NL}\right)^T \boldsymbol{Z}_{nl}^T \right\} \times \bar{\boldsymbol{Q}} \left\{ \boldsymbol{Z}_l \left(\boldsymbol{B}^L + \boldsymbol{B}^*\right) + \boldsymbol{Z}_{nl} \boldsymbol{B}^{NL} \right\} \right] dz dA \tag{15}$$

Readers are referred to Ref. [8] for complete derivation of K_σ. The convergence of the result is checked using both the relative displacement norm criteria, $\frac{\|\Delta q\|}{\|q\|} < \beta$, and residual normal criteria with error tolerance $\beta = 10^{-2}$.

The above procedure is valid for a single solution path. However, in bifurcation problems or buckling analysis, a primary solution path is bifurcated into a secondary path. A branch-switching technique [37,38] is generally preferred to trace the secondary or post-buckling path of composite plates. The solution point where the branch-switching technique is applied can be obtained by the change in the sign of the determinant of the tangent stiffness matrix with respect to the previous solution point. This branch-switching technique is applied at both primary and secondary bifurcation points in the present study. Further, only one post-buckling path is traced because the post-buckling response of the plate is symmetrically stable. The nonlinear eigenvalue approach is also used to trace the post-buckling path as explained in Ref. [43]. The two types of analyses undertaken in this study are summarized in the following subsection for clarity.

2.7.1. Linear buckling analysis due to in-plane mechanical loads

The linear buckling analysis due to in-plane mechanical loads is a two-step process. First, a unit load is applied to calculate the stress-resultant to be used in the second stage. Then, a scaled value is obtained using an eigenvalue problem.

Step 1: Pre-buckling analysis. For assumed uniform in-plane stress distribution, stress resultants are assumed to be equal to the applied in-plane loads P_i. For nonuniform in-plane stress distribution

$$\left(\boldsymbol{K}_1 + \gamma \boldsymbol{K}_\gamma\right) \boldsymbol{q}_s = \boldsymbol{F}_{P_i}$$

where

$$\boldsymbol{K}_1 = \int_V \left(\left(\boldsymbol{B}^L\right)^T \boldsymbol{Z}_l^T \bar{\boldsymbol{Q}} \boldsymbol{Z}_l \left(\boldsymbol{B}^L\right) \right) dz dA$$

Step 2: Bifurcation analysis.

$$\left(\boldsymbol{K}_1 + \gamma \boldsymbol{K}_\gamma\right) \boldsymbol{q}_d - \lambda \boldsymbol{K}_\sigma \left(\boldsymbol{q}_s\right) \boldsymbol{q}_d = 0$$

where $\boldsymbol{q}_d$ is the mode shape corresponding to the eigenvalue (or buckling load) and $\boldsymbol{K}_\sigma \left(\boldsymbol{q}_s\right)$ is the geometric stiffness matrix. The stress-resultants used in $\boldsymbol{K}_\sigma \left(\boldsymbol{q}_s\right)$ are defined by linear stress–strain relationship. The derivation of $\boldsymbol{K}_\sigma \left(\boldsymbol{q}_s\right)$ is given in Ref. [8]. The critical buckling load is obtained as the product of the critical load multiplier λ and the base load, i.e., the unit load in the pre-buckling analysis.

2.7.2. Nonlinear buckling analysis due to in-plane mechanical loads

The nonlinear buckling analysis due to in-plane mechanical loads is determined by solving the equation

$$\left(\boldsymbol{K} + \gamma \boldsymbol{K}_\gamma\right) \boldsymbol{q} = \lambda \boldsymbol{F}_{P_i}$$

where λ is a scale factor or load multiplier and $\boldsymbol{F}_{P_i}$ is the force vector due to a unit applied in-plane load. The critical value of λ is that value at which $det\left(K_T\right) = 0$.

It is worth mentioning that while some aspects of the mathematical formulation are common with those in [8], the present work is on the buckling of laminated composite plates with and without imperfections while the study in [8] is on bending. Also, the present study uses an extra HSDT model.

3. Results and discussions

In this section, a comparative study is conducted with the different buckling approaches to predict the buckling characteristics of laminated composite plates using the penalty based C^0 FEM-NPSDT model for different C^1 HSDTs. To account for stress stiffening effect due to in-plane mechanical loads, both von Kármán and Green–Lagrange type nonlinearities are used and compared to improve the understanding of the reliability of the different approaches. Buckling characteristics using these approaches are obtained and compared comprehensively for a variety of problems. The accuracy and efficacy of the present C^0 FE formulation are initially assessed with benchmark problems, and then a parametric study is implemented to investigate the influence of various parameters. To accomplish this, a MATLAB program is developed based on the procedure outlined in the Section 2. Three plate theories are considered, namely, (a) inverse hyperbolic shear deformation theory (IHSDT) [44] with $f(z) = sinh^{-1}(3z/h) - 6z/\left(h\sqrt{13}\right)$, (b) inverse hyperbolic tangent shear deformation theory (IHTSDT) [45] with $f(z) = tanh^{-1}(0.088z/h) - 0.088(z/h)/\left(1 - 0.088^2/4\right)$, and (c) third-order shear deformation theory (TSDT) [7] with $f(z) = z - 4z^3/3h^2$. The chosen NPSDTs, i.e., IHSDT and IHTSDT, are selected based on their analytical and numerical superior performance over the other theories as reported in the literature [44,45].

The present buckling analysis of composite plates is classified as either linear or nonlinear analysis. The obtained finite element (FE) results are validated using results in the literature along with Navier solutions and results from ANSYS simulations. The Navier solution

Table 1
Material properties used for the buckling analysis of laminated composite plates.

Material	E_1 (GPa)	E_2 (GPa)	G_{12} (GPa)	G_{13} (GPa)	G_{23} (GPa)	ν_{12}
MM1 [7,46,47]	$25E_2$ or Specified	1	$0.5E_2$	$0.5E_2$	$0.2E_2$	0.25
MM2 [7]	$40E_2$ or Specified	1	$0.6E_2$	$0.6E_2$	$0.5E_2$	0.25

for linear buckling analysis is based on uniform stress assumption, i.e., assumed stress approach. The mathematical formulation for the Navier solution for both uniaxial and biaxial compression is given in Appendix. Regarding ANSYS simulations, a SHELL281 shell element with a 24 × 24 mesh is considered for the linear analysis while a 12 × 12 mesh is considered for the nonlinear analysis. To trigger the post-buckling response in ANSYS MECHANICAL APDL18.1, the FE mesh is initially detached from the solid model; then, each node is augmented with the desired imperfection to conduct a nonlinear static analysis. The post-buckling equilibrium path is traced for a sinusoidal type of imperfection with amplitude $w_0^* = 10^{-5}$.

In subsequent examples, unless specified otherwise, all the (converged) FE solutions are obtained using a 12 × 12 element mesh for validation, comparison, and parametric study. For numerical calculations, a nine-node isoparametric element that is integrated using selective Gauss–Legendre quadrature rules – 3 × 3 Gauss–Legendre quadrature rule for linear bending stiffness and force vector, and 2 × 2 Gauss–Legendre quadrature rule for linear transverse stiffness and all remaining terms – is used.

3.1. Material properties

The two sets of material properties employed are tabulated in Table 1. The layers of the laminated plates have identical material and geometric properties.

3.2. Boundary conditions

Given that the formulation is based on a displacement approach with C^0 continuity, only kinematics boundary conditions, i.e., (u_0, v_0, w_0, ϕ_x, ϕ_y, θ_x, θ_y), are enforced. The different types of boundary conditions used are listed as follows:

- Pre-buckling
  $w_0 = \theta_x = \phi_x = 0$ at $y = 0, b$; $w_0 = \theta_y = \phi_y = 0$ at $x = 0, a$ for simply supported constraints
  $w_0 = \theta_x = \phi_x = \theta_y = \phi_y = 0$ at $y = 0, b$ and $x = 0, a$ for clamped constraints
  Tying conditions: $u_0 = v_0 = 0$ at $(x = 0, y = b/2)$ and $v_0 = 0$ at $(x = a, y = b/2)$ for rigid body constraint
  Tying conditions are used to restrict rigid motion in the pre-buckling analysis. The tying conditions used herein are taken from Ref. [24].
- Simply supported, SSSS

$u_0 = w_0 = \theta_x = \phi_x = 0$ at $y = 0, b$ and $v_0 = w_0 = \theta_y = \phi_y = 0$ at $x = 0, a$

- Clamped, CCCC

$u_0 = v_0 = w_0 = \theta_x = \theta_y = \phi_x = \phi_y = 0$ at $y = 0, b$ and $x = 0, a$

- ABFD A at

A at $y = 0$, B at $x = b$, no condition (free) at $y = b$, D at $x = 0$

3.3. Linear buckling analysis

A linear buckling analysis is implemented to validate the present C^0 FEM-HSDT formulation. Navier type analytical solutions are obtained for IHSDT, IHTSDT, TSDT and they are used to calibrate the value of the penalty parameter γ which is used in C^0 FEM-HSDT for C^1 HSDT. Further, linear buckling results using unconstrained third-order shear deformation theory (UTSDT) are also obtained to compare the accuracy of the aforementioned theories [24]. A unit edge load, more specifically, unit stress resultant $\boldsymbol{N}$ is applied to obtain the geometric stiffness matrix. Note that the edge load or in-plane load is a distributed line load (or stress resultant) along the edge.

The initial buckling strength of the laminated composite plate is calculated by solving an eigenvalue problem using an in-house MATLAB code and also via ANSYS simulation. To build the geometric stiffness matrix K_σ for linear buckling analysis, a linear static analysis is firstly conducted using appropriate boundary conditions to obtain the stress distribution. The different buckling approaches employed in this study – assumed stress, pre-buckling and linear buckling – are named according to the boundary conditions considered in the linear static analysis. The approach in which uniform stress distribution is assumed is named as assumed stress approach; pre-buckling approach when pre-buckling boundary condition is used in the linear static analysis; and linear buckling approach when the boundary condition is identical to that used in the eigenvalue analysis.

3.3.1. Simply supported thin rectangular isotropic plate

The proposed C^0 FEM-HSDT formulation is first validated using a simply supported (SSSS) thin $(b/h = 100)$ rectangular isotropic plate whose Young's modulus of elasticity $E = 1$ GPa and Poisson's ratio $\nu = 0.25$, and the penalty parameter $\gamma = 10^7$. The plate is subjected to different types of uniaxial loads as depicted in Fig. 3. A normalized buckling load $\bar{P} = \frac{Pb^2}{\pi^2 D}$, where $D = \frac{Eh^3}{12(1-\nu^2)}$, is employed for comparison purposes. Table 2 presents the values of the normalized buckling load $\bar{P}$ obtained using ANSYS and using the C^0 FEM-TSDT model for both von Kármán and Green–Lagrange nonlinearities, and solutions in the literature. The present C^0 FEM-TSDT results are in good agreement with ANSYS results, FEM-UTSDT solutions of Adhikari and Singh [24], and TSDT solutions of Panda and Ramachandra [48].

It is also observed that loading patterns with more concentration around the corner, i.e., inverse triangular and inverse sinusoidal, yield higher buckling load than those with concentration at the center. This may be attributed to the immovable boundary condition of the four corner points. Further, no significant difference is observed in the values of buckling load $\bar{P}$ for both von Kármán and Green–Lagrange nonlinearities (or stress stiffening) because of the thinness of the plate $(b/h = 100)$. For completeness, the corresponding buckling modes are shown in Fig. 4, where it is observed that the plate with an exact ratio $a/b = 3$ buckled in the third mode (with respect to mode shapes of a square plate). Finally, it is noted that penalty parameter does not have a material effect because of the thinness of the plate.

3.3.2. Effect of penalty parameter (γ)

The value of the penalty parameter $(\gamma = 10^9)$ employed in the previous example was based on a bending analysis study [8]. It is, however, worthwhile to assess the effect of the penalty parameter γ on the present C^0 FEM-HSDT solutions. The assessment is limited to the von Kármán nonlinearity, and it is based on a simply supported (SSSS) square cross-ply laminated plate that is subjected to (uniform) uniaxial loads. Material MM1 [7] (see Table 1) is employed and the normalized buckling load is calculated as $\bar{P} = Pb^2/E_2h^3$. Table 3 shows FE results obtained using NPSDT, UTSDT, and ANSYS for pre-buckling approach, and Navier solutions using assumed stress approach. The FE solutions show that an accurate prediction of critical buckling is dependent on the penalty parameter. Compared to the value of the penalty parameter used in the bending analysis study [8], the C^0 FEM-NPSDT buckling analysis requires a higher penalty value $\gamma = 10^{12}$. Further, the effect of

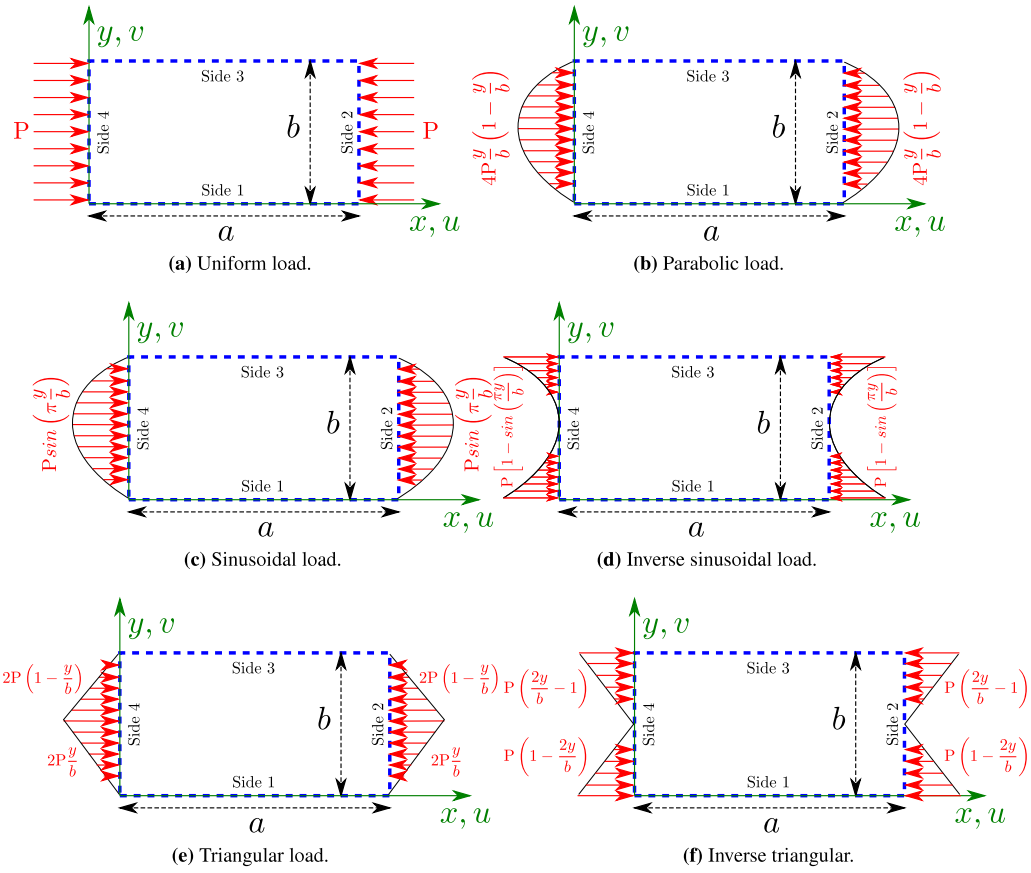

(a) Uniform load. **(b)** Parabolic load.

(c) Sinusoidal load. **(d)** Inverse sinusoidal load.

(e) Triangular load. **(f)** Inverse triangular.

Fig. 3. Different types of uniaxial compression load.

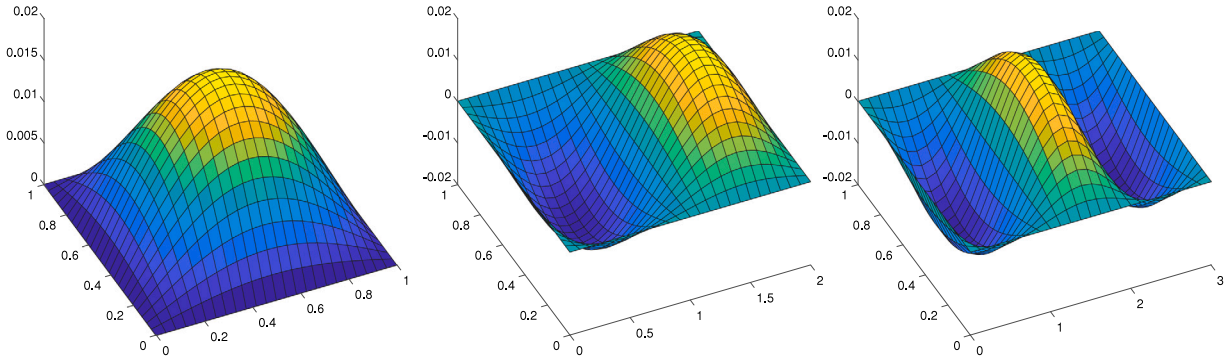

(a) $a/b = 1$. **(b)** $a/b = 2$. **(c)** $a/b = 3$.

Fig. 4. Buckling modes of simply supported (SSSS) thin ($b/h = 100$) rectangular isotropic plate subjected to uniaxial loads with different aspect ratio, a/b.

the penalty parameter decreases with increasing a/h ratio. The present FE results without penalty ($\gamma = 0$) are lower than the Navier solutions, FEM-NPSDT results with penalty ($\gamma = 10^{12}$), and UTSDT, which is better with respect to ANSYS solutions. The improvement is due to the C^0 FE implementation as an unconstrained higher-order shear deformation theory (UHSDT) with seven field variables (see Eq. (2)) in comparison to original traction free NPSDT with five field variables (see Eq. (1)). It uses UHSDT and allows material points to deform freely, hence yields a softer stiffness matrix in comparison to the present NPSDT. Also, the accuracy of the IHSDT and IHTSDT is good for both symmetric and anti-symmetric cross-ply laminated plates. Therefore, a comprehensive study is needed to demonstrate the effectiveness of any new NPSDT model for buckling analysis. In particular, the accuracy of IHTSDT is found to be the same as that of TSDT. In other words, IHTSDT can be viewed as an equivalent non-polynomial form of TSDT. Since the present study is based on C^1 HSDT, it is important to consider the role of penalty stiffness in the FE formulations for accurate predictions of buckling load, where accuracy is measured by the proximity to the Navier solution of C^1 NPSDT.

3.3.3. *Effect of pre-buckling boundary condition*

Two sets of boundary conditions are used in the calculation of the critical buckling load: firstly, during the pre-buckling analysis or linear static analysis; and secondly, during the linear eigenvalue analysis. Generally, pre-buckling analysis is performed to determine the pre-buckling stress distribution for use in the geometric stiffness matrix

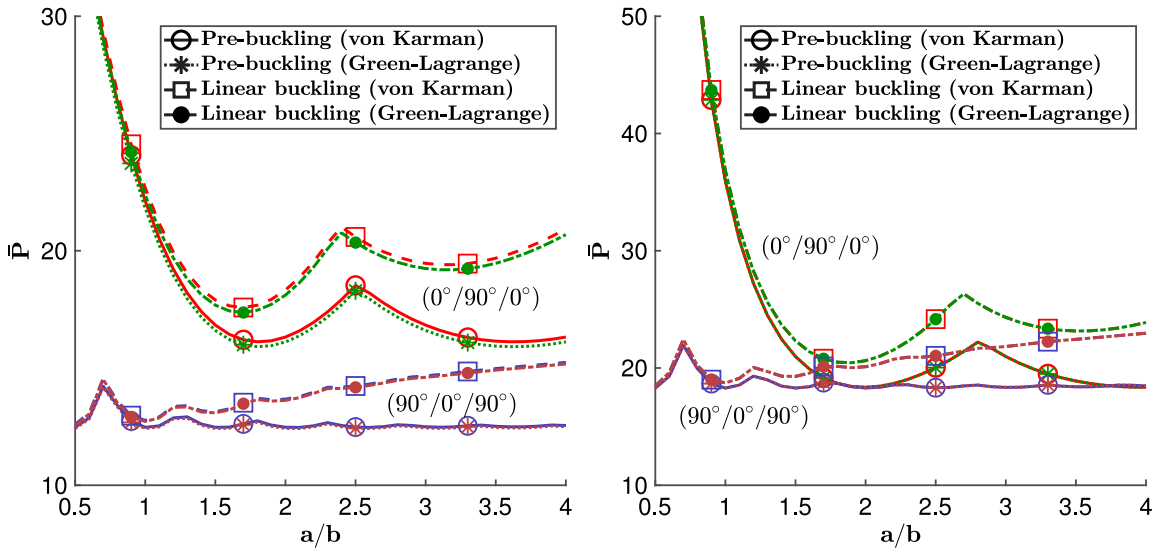

(a) $a/h = 10$. **(b)** $a/h = 100$.

Fig. 5. Effect of aspect ratio (a/b) on normalized buckling load $\left(\bar{P} = Pb^2/E_2h^3\right)$ of simply supported (SSSS) cross-ply $(0°/90°/0°)$ and $(90°/0°/90°)$ laminated plates under uniaxial loads.

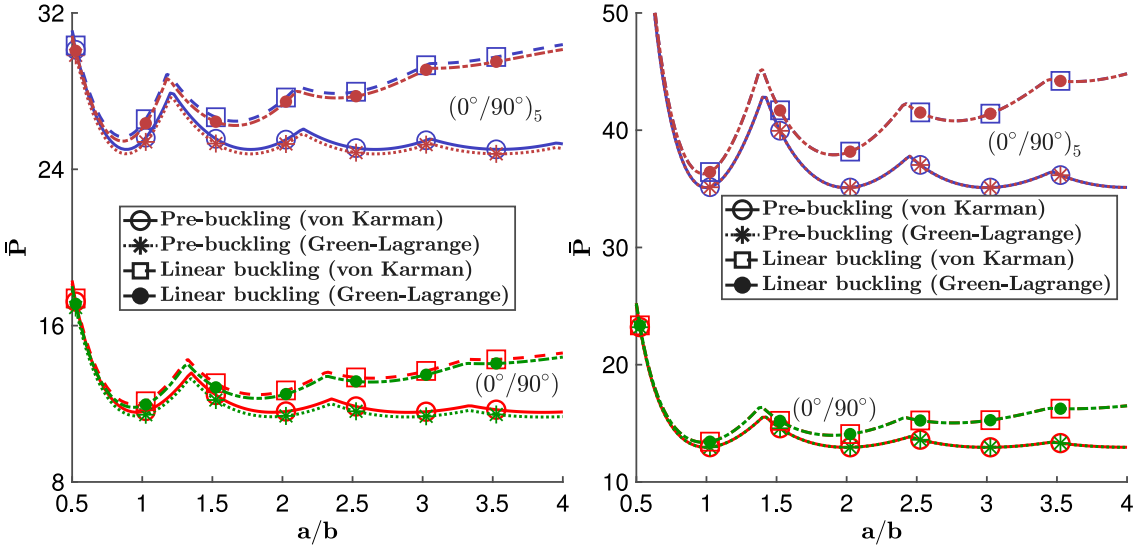

(a) $a/h = 10$. **(b)** $a/h = 100$.

Fig. 6. Effect of aspect ratio (a/b) on normalized buckling load $\left(\bar{P} = Pb^2/E_2h^3\right)$ of simply supported (SSSS) cross-ply $(0°/90°)$ and $(0°/90°)_5$ laminated plates under uniaxial loads.

to capture stress stiffening effect. However, the use of pre-buckling boundary condition (see Section 3.2) yields approximately the same stress distribution as that used in the assumed uniform stress approach. A superior design and analysis of composite plates requires the use of identical boundary conditions in both pre-buckling and linear eigenvalue analyses since nonlinear buckling approach uses only a single set of boundary conditions (see Section 3.4).

The effect of pre-buckling boundary is investigated using a simply supported (SSSS), moderately thick $(a/h = 10)$ square cross-ply laminated plate that is made of material MM2 [7] (see Table 1) and subjected to uniform uniaxial loads. A comparative analysis is performed between the pre-buckling approach and linear buckling approach for UTSDT, IHTSDT, and IHSDT, and the results are tabulated in Table 4. It is observed that buckling loads based on the linear buckling approach (i.e., consistent boundary conditions in both pre-buckling and linear eigenvalue analysis) are higher than those obtained using the pre-buckling approach or assumed stress approach. These higher buckling loads can be attributed to immovable corner points which cause non-uniform stress distribution. This observation is corroborated by ANSYS simulation results.

Table 4 indicates that the buckling load increases with increasing modulus ratio (E_1/E_2) and it can be attributed to increasing bending stiffness of the plate. The IHTSDT yields lower and more accurate results than IHSDT based on the proximity of its solutions to corresponding ANSYS solutions. Collectively, the relative error between solutions obtained using von Kármán and Green–Lagrange stress stiffening is approximately 3% in all cases. The relative error is calculated with respect to Green–Lagrange solutions. In conclusion, the buckling analysis using Green–Lagrange nonlinearity yields lower, reliable, and conservative results compared to using von Kármán nonlinearity. This improvement can be attributed to the higher stiffening exhibited by Green–Lagrange nonlinearity due to the contribution of in-plane displacements. It is worth observing that the present Green–Lagrange-based geometric stiffness matrix is not determined with a pre-assumed

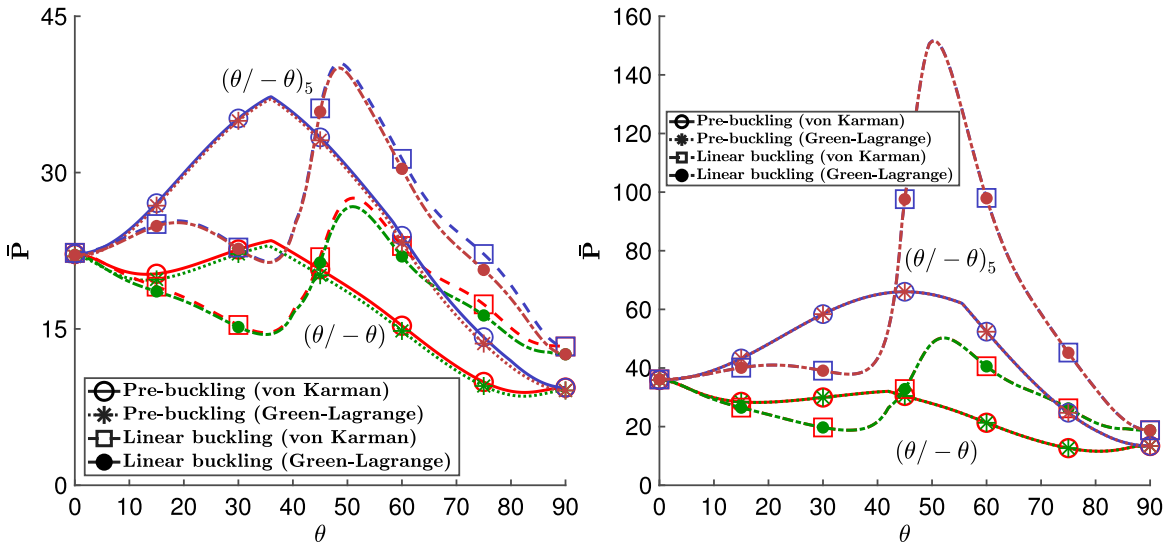

(a) $a/h = 10$. **(b)** $a/h = 100$.

Fig. 7. Effect of fiber orientation (θ) on normalized buckling load ($\bar{P} = Pb^2/E_2h^3$) of simply supported (SSSS) angle-ply $(\theta/-\theta)$ and $(\theta/-\theta)_5$ square laminated plates under uniaxial loads.

Table 2
Critical buckling load ($\bar{P}$) of simply supported (SSSS) thin ($b/h = 100$) isotropic plate subjected to different types of uniaxial loads.

a/b	Source/Model	Nonlinearity	Uniform[a,b]	Parabolic[b]	Triangular[b]	Inverse triangular[b]	Sinusoidal[b]	Inverse sinusoidal[b]
1/3	FEM-TSDT	von Kármán	11.0821	12.6368	15.4033	31.0602	12.9072	47.8871
	FEM-TSDT	Green–Lagrange	11.0730	12.6268	15.3911	31.0291	12.8970	47.8305
	ANSYS		11.0820	12.6878	15.9273	30.9760	12.9640	47.4920
1	FEM-UNTSDT [24]	von Kármán	3.9979	5.2395	–	–	–	–
	TSDT [48]		3.9970	5.2410	–	–	–	–
	FEM-TSDT		3.9979	5.2394	6.6753	9.8626	5.4161	14.9544
	FEM-TSDT	Green–Lagrange	3.9973	5.2387	6.6744	9.8606	5.4153	14.9509
	ANSYS [24]		3.9553	5.1978	–	–	–	–
	ANSYS		3.9978	5.2542	6.6876	9.8381	5.4315	14.845
3	FEM-UNTSDT [24]	von Kármán	3.9993	5.6315	–	–	–	–
	TSDT [48]		3.9970	5.5470	–	–	–	–
	FEM-TSDT		3.9981	5.6292	7.2982	8.3689	5.8540	11.6238
	FEM-TSDT	Green–Lagrange	3.9976	5.6298	7.2969	8.3674	5.8531	11.6216
	ANSYS [24]		3.9781	5.5967	–	–	–	–
	ANSYS		3.9980	5.6410	7.3013	8.3655	5.8605	11.5900

[a] Denote present solutions using assumed stress approach.
[b] Denote present solutions using assumed pre-buckling approach.

uniform in-plane stress distribution as commonly found in the literature [4,14,15,24]. The present FE model can be used for any composite plate with any type of in-plane loading and boundary conditions.

3.3.4. *Effect of boundary conditions*

The effect of different boundary conditions on buckling characteristics of laminated composite plates is investigated using the present C^0 FEM-TSDT model. A four layer $(0°/90°/90°/0°)$ square laminated plate under different combinations of simply supported (S), clamped (C) and free (F) boundary condition are considered. Material MM2 [7] is used for all layers (as given in Table 1), and two types of in-plane load configurations are considered: Case-1 (compression along x-axis) and Case-2 (compression along both x-axis and y-axis). The normalized buckling loads $\bar{P} = Pb^2/E_2h^3$ for $a/h = 10$ are tabulated in Tables 5 to 7 for both pre-buckling and linear buckling approaches. Using ANSYS solutions as benchmark, it is observed that the use of Green–Lagrange stiffening yields lower and more accurate results compared to the results obtained using von Kármán stiffening. The linear buckling approach predicts lower buckling load in comparison to pre-buckling approach for plates with free boundary edges, which indicates lower strength exhibited by the structures. Particularly for CCCC, FCCC, FCFC, SCCC, and SCSC boundary conditions, the pre-buckling approach gives unrealistic results as these conditions do not display buckling as evident from linear buckling approach. This can be confirmed from the linear buckling approach which includes the clamped boundary condition in pre-buckling analysis.

3.3.5. *Effect of aspect ratio* (a/b)

The effect of aspect ratio a/b on the buckling strength of rectangular laminated composite plates is investigated using four different types of cross-ply laminated plates $(0°/90°/0°)$, $(90°/0°/90°)$, $(0°/90°)$ and $(0°/90°)_5$ that are subjected to uniaxial loads. Material MM2 (see Table 1) is used as material property for all layers. The normalized buckling load $\bar{P} = Pb^2/E_2h^3$ obtained via FEM-TSDT model for composite plates having $a/h = 10$ and 100 are depicted in Figs. 5 and 6. The solutions obtained using the linear buckling approach show a linearly varying stiff response with increase in aspect ratio a/b, than the response based on the pre-buckling approach. This behavior may be attributed to non-uniform stress distribution caused by the immovable corner points of the plate. Further, for moderately thick plate $(a/h = 10)$, the noticeable difference in the normalized buckling load $\bar{P}$ in results obtained using Green–Lagrange and von Kármán stiffening

Table 3
Normalized buckling load ($\bar{P}$) of simply supported (SSSS) square laminated plate under uniform uniaxial loads.

Lamination	a/h	ANSYS	CFS				FES	$\gamma = 10^{12}$		$\gamma = 0$	
			UTSDT[a]	TSDT[a]	IHTSDT[a]	IHSDT[a]	UTSDT[b]	TSDT[b]/ IHTSDT[b]	IHSDT[b]	TSDT[b]/ IHTSDT[b]	IHSDT[b]
(0°/90°/0°)	6	7.8242	8.6752	8.7322	8.7330	8.4557	8.6797	8.7330	8.4558	8.6759	8.4477
	8	10.7960	11.6886	11.7775	11.7784	11.4056	11.6922	11.7785	11.4057	11.6895	11.3934
	10	13.2670	14.1201	14.2205	14.2215	13.8256	14.1237	14.2217	13.8258	14.1210	13.8085
	20	19.5820	20.0338	20.0987	20.0993	19.8611	20.0378	20.0996	19.8614	20.0345	19.8458
	50	22.7590	22.8554	22.8698	22.8700	22.8177	22.8581	22.8704	22.8181	22.8559	22.8142
	100	23.3060	23.3314	23.3352	23.3353	23.3215	23.3332	23.3357	23.3220	23.3319	23.3209
$(0°/90°)_s$	6	N/A	8.7304	8.8022	8.8030	8.6026	8.7394	8.8031	8.6026	8.7310	8.6023
	8	11.1820	11.6830	11.7842	11.7851	11.5299	11.6897	11.7852	11.5300	11.6837	11.5283
	10	13.6050	14.0650	14.1760	14.1769	13.9095	14.0716	14.1770	13.9097	14.0658	13.9060
	20	19.7190	19.9516	20.0226	20.0231	19.8612	19.9592	20.0234	19.8615	19.9522	19.8570
	50	22.7850	22.8337	22.8496	22.8498	22.8138	22.8389	22.8502	22.8142	22.8341	22.8130
	100	23.3130	23.3256	23.3298	23.3298	23.3204	23.3287	23.3303	23.3208	23.3260	23.3205
(0°/90°)	6	6.5180	6.7291	6.8253	6.8250	7.0360	6.7836	6.8861	7.1001	6.8348	6.8836
	8	7.5510	7.7189	7.7854	7.7852	7.9330	7.7532	7.8239	7.9722	7.7902	7.8261
	10	8.1561	8.2841	8.3315	8.3313	8.4373	8.3078	8.3584	8.4643	8.3352	8.3616
	20	9.1480	9.1819	9.1958	9.1957	9.2270	9.1950	9.2104	9.2417	9.2043	9.2126
	50	9.4740	9.4696	9.4719	9.4719	9.4772	9.4821	9.4849	9.4903	9.4842	9.4858
	100	9.5224	9.5122	9.5128	9.5128	9.5141	9.5245	9.5254	9.5268	9.5253	9.5258
$(0°/90°)_2$	6	6.5897	6.9194	10.1001	10.1003	10.1281	8.8611	9.5737	9.7567	9.5657	9.5651
	8	10.4910	12.4168	12.8711	12.8713	12.8784	12.4232	12.8834	12.8902	12.8789	12.8570
	10	12.9860	14.3682	14.7580	14.7582	14.7569	14.3730	14.7682	14.7670	14.7633	14.7431
	20	17.6200	18.2103	18.3663	18.3664	18.3621	18.2120	18.3718	18.3680	18.3696	18.3611
	50	19.5810	19.6923	19.7214	19.7214	19.7204	19.6944	19.7252	19.7244	19.7249	19.7235
	100	19.8980	19.9243	19.9317	19.9317	19.9315	19.9268	19.9351	19.9349	19.9351	19.9348

[a] Present closed form solutions (CFS) using Navier approach.
[b] Present finite element solutions (FES) using pre-buckling approach.

Table 4
Effect of pre-buckling boundary condition on the critical buckling load ($\bar{P} = Pb^2/E_2h^3$) of simply supported (SSSS) square laminated plates with $a/h = 10$.

Lamination	E_1/E_2	von Kármán nonlinearity													Green–Lagrange nonlinearity										
		IHSDT [44]	UTSDT[a]	TSDT[a]	IHSDT[a]	UTSDT[b]	UTSDT[c]	UTSDT[d]	IHTSDT[b]	IHTSDT[c]	IHTSDT[d]	IHSDT[b]	IHSDT[c]	IHSDT[d]	UTSDT[b]	UTSDT[c]	UTSDT[d]	TSDT[b]	TSDT[c]	TSDT[d]	IHSDT[b]	IHSDT[c]	IHSDT[d]	ANSYS[c]	ANSYS[d]
(0°/90°/0°)	3	–	5.3896	5.3898	5.3949	5.3897	5.3968	6.7934	5.3899	5.3899	6.7899	5.3950	5.3950	6.7965	5.3122	5.3139	6.6938	5.3125	5.2898	6.6620	5.3173	5.2945	6.6682	5.3878	6.7875
	10	–	9.8319	9.8325	9.8503	9.8321	9.8408	10.7857	9.8327	9.8327	10.7767	9.8504	9.8504	10.7962	9.7043	9.6897	10.6323	9.7048	9.6535	10.5889	9.7220	9.6702	10.6073	9.8174	10.7610
	20	–	14.8882	14.8896	14.9415	14.8884	14.8945	15.6486	14.8899	14.8899	15.6349	14.9417	14.9417	15.6894	14.7156	14.6915	15.4540	14.7170	14.6437	15.3917	14.7677	14.6934	15.4440	14.8390	15.5830
	30	–	18.8750	18.8776	18.9750	18.8753	18.8792	19.5271	18.8778	18.8779	19.5105	18.9752	18.9752	19.6111	18.6746	18.6496	19.3121	18.6773	18.5905	19.2325	18.7729	18.6848	19.3300	18.7780	19.4093
	40	–	22.1164	22.1207	22.2704	22.1166	22.1194	22.6935	22.1210	22.1211	22.6753	22.2707	22.2707	22.8287	21.8975	21.8761	22.4687	21.9020	21.8063	22.3740	22.0494	21.9519	22.5234	21.9600	22.5136
$(0°/90°)_s$	3	5.4002	5.3932	5.3933	5.4002	5.3933	5.4039	7.2403	5.3934	5.3934	7.23287	5.4003	5.4003	7.2427	5.3159	5.3129	7.1199	5.3160	5.2832	7.0762	5.3226	5.2896	7.0852	5.3905	7.2291
	10	9.9741	9.9392	9.9406	9.9741	9.9393	9.9552	11.3007	9.9407	9.9406	11.2806	9.9742	9.9742	11.3191	9.8111	9.7771	11.1123	9.8126	9.7305	11.0494	9.8452	9.7619	11.0852	9.9108	11.2470
	20	15.3936	15.2900	15.2984	15.3936	15.2902	15.3020	16.3924	15.2986	15.2980	16.3671	15.3938	15.3938	16.4698	15.1169	15.0540	16.1502	15.1255	15.0042	16.0702	15.2189	15.0948	16.1672	15.2080	16.2720
	30	19.8413	19.6537	19.6744	19.8413	19.6539	19.6610	20.6109	19.6746	19.6730	20.5884	19.8416	19.8416	20.7650	19.4541	19.3756	20.3406	19.4750	19.3302	20.2523	19.6395	19.4905	20.4201	19.5060	20.4150
	40	23.5796	23.3026	23.3400	23.5795	23.3029	23.3065	24.1601	23.3403	23.3403	24.1460	23.5798	23.5798	24.3970	23.0869	23.0019	23.8764	23.1248	22.9652	23.7866	23.3612	23.1963	24.0257	23.0780	23.8800
$(0°/90°)_1$	3	–	4.7748	4.7749	4.7827	4.7749	4.7870	6.4093	4.7750	4.7885	6.4103	4.7827	4.7964	6.4216	4.6881	4.7159	6.3234	4.6882	4.7049	6.2998	4.6956	4.7124	6.3105	4.7818	6.3992
	10	–	6.2585	6.2721	6.2964	6.2587	6.2788	7.1456	6.2722	6.2950	7.1624	6.2965	6.3196	7.1910	6.1217	6.1705	7.0459	6.1352	6.1737	7.0456	6.1584	6.1968	7.0727	6.2173	7.0767
	20	–	8.0439	8.1151	8.1714	8.0440	8.0643	8.6695	8.1152	8.1380	8.7480	8.1716	8.1945	8.8098	7.8641	7.9280	8.5523	7.9357	7.9874	8.6142	7.9884	8.0406	8.6731	7.8903	8.4911
	30	–	9.7004	9.8695	9.9669	9.7005	9.7224	10.2296	9.8695	9.8941	10.4101	9.9671	9.9913	10.5142	9.4862	9.5654	10.0968	9.6536	9.7210	10.2595	9.7466	9.8131	10.3592	9.4128	9.9182
	40	–	11.2604	11.5625	11.7094	11.2606	11.2853	11.7405	11.5625	11.5902	12.0584	11.7096	11.7365	12.2131	11.0771	11.1117	11.5946	11.3160	11.3987	11.8931	11.4563	11.5379	12.0418	10.8236	11.2790
$(0°/90°)_5$	3	–	5.3875	5.3882	5.3959	5.3876	5.3877	7.2174	5.3883	5.3888	7.2184	5.3960	5.3966	7.2294	5.3094	5.3235	7.1395	5.3100	5.3109	7.1136	5.3174	5.3183	7.1241	5.3823	7.2097
	10	–	10.0443	10.0557	10.0825	10.0445	10.0444	11.3996	10.0559	10.0570	11.4127	10.0827	10.0837	11.4433	9.9120	9.9343	11.2896	9.9233	9.9264	11.2755	9.9489	9.9520	11.3049	10.0165	11.3682
	20	–	15.8699	15.9141	15.9829	15.8702	15.8703	16.9828	15.9144	15.9158	17.0302	15.9832	15.9846	17.1039	15.6884	15.7219	16.8415	15.7323	15.7376	16.8541	15.7985	15.8038	16.9252	15.7995	16.9088
	30	–	20.8961	20.9864	21.1103	20.8964	20.8968	21.8732	20.9867	20.9884	21.9678	21.1106	21.1123	22.0975	20.6867	20.7297	21.7162	20.7766	20.7837	21.7689	20.8964	20.9034	21.8946	20.7747	21.7484
	40	–	25.2777	25.4225	25.6113	25.2781	25.2788	26.1591	25.4228	25.4248	26.3090	25.6116	25.6135	26.5043	25.0539	25.1046	25.9963	25.1983	25.2068	26.0986	25.3814	25.3898	26.2884	25.0998	25.9779

[a] Present closed form solutions (CFS) for assumed uniform stress distribution using Navier approach.
[b] Represents present finite element solutions (FES) using assumed stress approach.
[c] Represents present finite element solutions (FES) using pre-buckling approach.
[d] Represents present finite element solutions (FES) using linear buckling approach.

support the use of Green–Lagrange nonlinearity. While an identical behavior was also observed by Nima et al. [26] in their study using linear buckling approach, they considered slightly different in-plane constraints.

3.3.6. *Effect of fiber orientation* (θ)

The objective of this numerical simulation is to examine the influence of fiber orientation θ on the buckling strength of simply supported (SSSS) angle-ply laminated plates subjected to uniaxial loads. Two types of angle-ply laminated plates are considered, namely, $(\theta/-\theta)$ and $(\theta/-\theta)_5$. As in the previous problem, the set of material properties is Material MM2 (see in Table 1). The obtained normalized buckling loads $\bar{P} = Pb^2/E_2h^3$ for $a/h = 10$ and 100 are plotted in Fig. 7 using FEM-TSDT model for both pre-buckling and linear buckling approaches. It is observed that the optimal ply orientation for angle-ply laminated plates for $a/h = 10$ is $\theta = 36°$ with pre-buckling approach and $\theta = 50°$ with linear buckling approach. While for thin plate, $a/h = 100$, the optimal fiber orientation is around $\theta = 43°$ with pre-buckling approach and $\theta = 50°$ with linear buckling approach. These differences may be attributed to the non-uniform stress distribution developed in the pre-buckling analyses. Further, a noticeable difference is observed in the results obtained using Green–Lagrange and von Kármán stiffening for moderately thick plate ($a/h = 10$), once more supporting the use of Green–Lagrange nonlinearity model.

3.4. *Nonlinear buckling analysis*

Nonlinear buckling analyses with and without imperfection enhance the understanding of buckling response of composite plates. To switch from the primary solution path to the secondary solution path, a perturbation type simple path switching technique, as discussed in Section 2.7, is utilized in conjunction with the arc-length method. In addition to buckling strength, a nonlinear analysis provides a complete information of displacement in an unnormalized scale, which is not possible with a linear eigenvalue buckling analysis.

Table 5
Normalized buckling load ($\bar{P} = Pb^2/E_2h^3$) of square laminated $(0°/90°)_s$ plate subjected to different uniaxial and biaxial compression with $b/h = 10$.

Boundary conditions	Approach	Uniform		Parabolic		Sinusoidal		Inverse sinusoidal		Triangular		Inverse triangular	
		Case-1	Case-2	Case-1	Case-2	Case-1	Case-2	Case-1	Case-2	Case-1	Case-2	Case-1	Case-2
SSSS	Pre-buckling[a]	23.3403	11.6702	27.5850	13.8137	28.2715	14.1627	99.7645	54.0749	34.1317	17.1242	69.8997	35.4642
	Pre-buckling[b]	22.9652	11.5624	27.2653	13.7184	27.9529	14.0675	51.5390	52.9305	33.7726	17.0157	46.9414	34.9036
	ANSYS	23.0780	11.5390	27.3580	13.7000	28.0440	14.0480	53.7920	34.3698	33.8130	16.9610	50.6880	32.2810
	Linear buckling[a]	24.1491	12.0751	27.9517	13.9975	28.6269	14.3407	108.9450	57.3190	34.5290	17.3222	76.1742	38.2055
	Linear buckling[b]	23.7866	11.9721	27.6310	13.9036	28.3070	14.2466	74.4922	56.3384	34.1677	17.2146	63.4474	37.6575
	ANSYS	23.8800	11.9410	27.7370	13.8900	28.4110	14.2320	59.1840	38.2160	34.2220	17.1650	55.5340	35.5140
SSSF	Pre-buckling[a]	12.1013	3.6521	13.5066	5.4842	13.8042	5.7362	60.2550	9.8462	16.5425	7.2677	37.9931	7.2415
	Pre-buckling[b]	11.9699	3.6355	13.4176	5.4641	13.7170	5.7157	49.2291	9.7835	16.4478	7.2433	37.0792	7.1994
	ANSYS	11.7920	3.5335	13.2170	5.3144	13.5090	5.5571	51.1500	9.5082	16.1610	7.0317	36.3010	7.0076
	Linear buckling[a]	11.5749	3.6058	13.3685	5.4560	13.6792	5.7085	53.1014	9.5749	16.4220	7.2362	34.0880	7.0840
	Linear buckling[b]	11.4726	3.5914	13.2847	5.4372	13.5964	5.6893	52.0509	9.5257	16.3312	7.2131	33.5424	7.0496
	ANSYS	11.2790	3.4890	13.0690	5.2856	13.3750	5.5288	48.0160	9.2539	16.0320	6.9995	32.7300	6.8581
FSSS	Pre-buckling[a]	18.1243	7.3662	25.6276	9.2497	26.4574	9.4935	33.6833	24.4140	32.4366	11.4363	28.3054	17.4746
	Pre-buckling[b]	17.9573	7.2803	25.4090	9.1788	26.2320	9.4238	33.1888	23.9220	32.1628	11.3610	27.9141	17.1699
	ANSYS	18.0560	7.1925	25.5110	9.0214	26.3300	9.2577	33.6040	23.6860	32.2170	11.1280	28.2290	17.0660
	Linear buckling[a]	18.0568	7.2828	25.7671	9.2301	26.6094	9.4762	33.5402	23.3061	32.6454	11.4214	28.1381	16.8798
	Linear buckling[b]	17.8903	7.1970	25.5501	9.1584	26.3851	9.4057	33.0475	22.8412	32.3719	11.3449	27.7487	16.5885
	ANSYS	17.9890	7.1114	25.6540	8.9992	26.4860	9.2379	33.4590	22.6620	32.4310	11.1110	28.0620	16.5030
SFSF	Pre-buckling[a]	5.0635	2.8245	5.7360	4.2049	5.8721	4.3907	32.5114	7.8214	7.0834	5.5280	16.9211	5.7187
	Pre-buckling[b]	5.0135	2.8032	5.7048	4.1808	5.8420	4.3663	31.3469	7.7338	7.0520	5.4998	16.5345	5.6609
	ANSYS	4.8575	2.7107	5.5280	4.0403	5.6600	4.2177	30.1790	7.4864	6.8185	5.3033	16.0580	5.4867
	Linear buckling[a]	4.9134	2.7783	5.7045	4.1724	5.8447	4.3584	28.0496	7.5767	7.0587	5.4900	15.5033	5.5727
	Linear buckling[b]	4.8745	2.7604	5.6753	4.1504	5.8162	4.3360	27.4301	7.5099	7.0287	5.4641	15.2582	5.5269
	ANSYS	4.7264	2.6666	5.4939	4.0078	5.6300	4.1854	26.2810	7.2590	6.7913	5.2656	14.7550	5.3494
FSFS	Pre-buckling[a]	17.7566	7.1940	24.6772	8.7596	25.5214	8.9744	30.3519	22.4345	31.4479	10.7737	25.8586	16.3619
	Pre-buckling[b]	17.6621	7.1076	24.5129	8.6920	25.3485	8.9082	29.8568	22.0646	31.2280	10.7023	25.4141	16.1220
	ANSYS	17.6880	7.0174	24.5970	8.5591	25.4320	8.7700	30.3950	22.0130	31.2730	10.5130	25.8730	16.1170
	Linear buckling[a]	17.7567	7.1425	24.7557	8.7476	25.6112	8.9639	30.6693	21.6056	31.5826	10.7650	26.0485	15.8675
	Linear buckling[b]	17.6622	7.0557	24.5916	8.6793	25.4386	8.8970	30.1676	21.2503	31.3627	10.6928	25.5997	15.6360
	ANSYS	17.6880	6.9680	24.6740	8.5459	25.5200	8.7584	30.7030	21.2180	31.4080	10.5030	26.0590	15.6360

Case-1 : uniaxial compression; Case-2 : biaxial compression.

[a] Present FEM-TSDT solution using von Kármán nonlinearity.

[b] Present FEM-TSDT solution using Green–Lagrange nonlinearity.

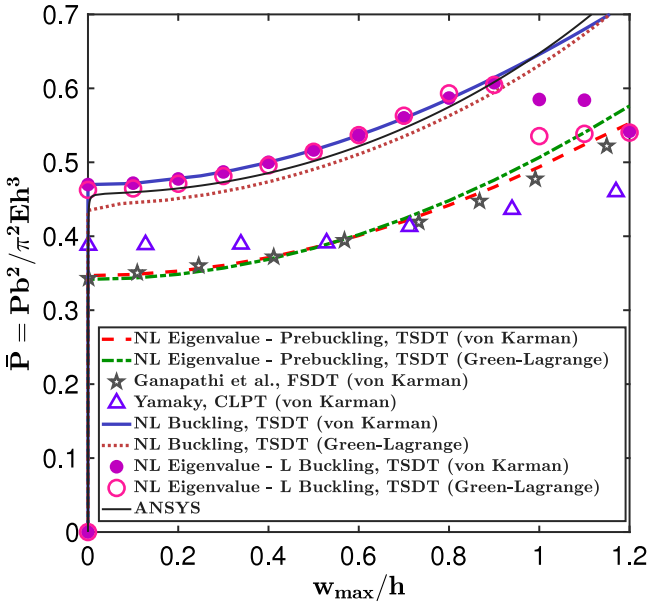

Fig. 8. Comparison of nonlinear eigenvalue approach and nonlinear buckling approach for buckling and post-buckling analyses of simply supported (SSSS) square isotropic plate under uniaxial loads with $a/h = 10$.

3.4.1. Simply supported isotropic plate

A comparative study is conducted on simply supported (SSSS) square isotropic plate subjected to (uniform) uniaxial load as considered in Section 3.3.1. The material properties are $E = 1$ GPa and $\nu = 0.3$. This problem was studied by Ganapathi et al. [49] (using FSDT) and Yamaky as cited in [49] (using CLPT) via a nonlinear eigenvalue approach that incorporate von Kármán nonlinearity. Fig. 8 shows the plots of the deflection-load response of a moderately thick plate $(a/h = 10)$ obtained using the present C^0 FEM-TSDT model along with ANSYS solution and the results reported in the literature. The present results are obtained using both the nonlinear eigenvalue approach and the nonlinear buckling approach, and they are identified with the labels NL Eigenvalue and NL Buckling, respectively.

For the nonlinear eigenvalue approach, a linear buckling analysis is initially conducted using the pre-buckling/linear buckling approach and followed by a nonlinear eigenvalue analysis (employing direct iterative technique as discussed in Ref. [43]) for SSSS boundary condition. The nonlinear eigenvalue solutions are labeled as “Prebuckling” and “L Buckling” for pre-buckling and linear buckling approaches, respectively (see Fig. 8). It is observed that the post-buckling response using nonlinear eigenvalue approach with pre-buckling is in good agreement with the FSDT results of Ganapathi et al. [49]. Further, the nonlinear eigenvalue approach using linear buckling approach is in good agreement with the nonlinear buckling approach, supporting the importance for a realistic or consistent boundary condition in the linear buckling analysis. The substantial difference observed in Fig. 9 for stress variation between nonlinear buckling analysis using FEM-TSDT and ANSYS simulation results supports the need of higher-order shear deformation model. Further, a considerable difference is observed

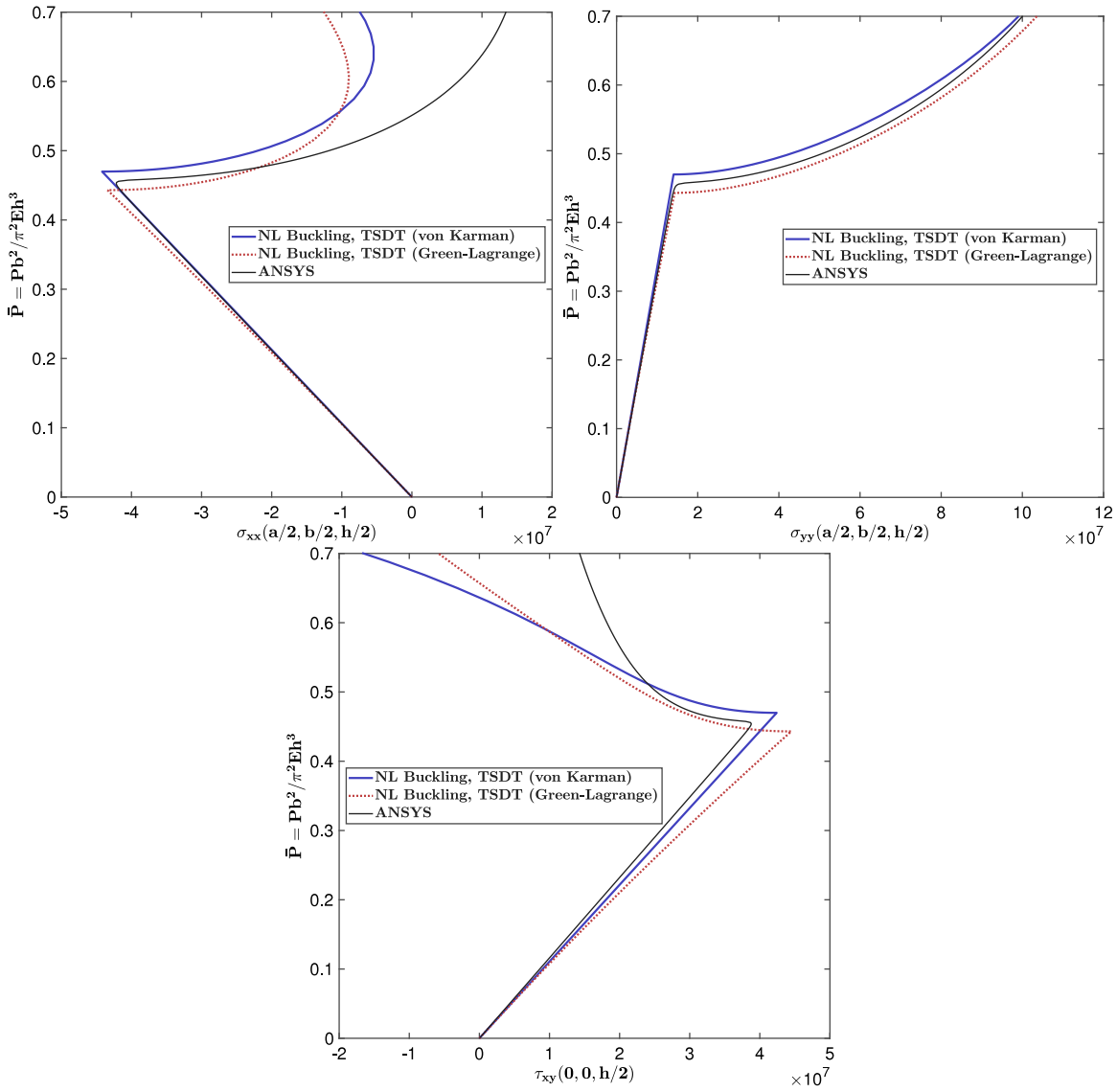

Fig. 9. Variation of stresses at critical points for buckling and post-buckling analyses of simply supported (SSSS) square isotropic plate under uniaxial loads with $a/h = 10$.

between results based on von Kármán and Green–Lagrange nonlinearities following nonlinear buckling approach. Thus highlighting the importance of Green–Lagrange nonlinearity in the design and analysis. It is clear from Fig. 8 that the nonlinear buckling approach is superior to the nonlinear eigenvalue approach, probably because the entire problem is solved with a single boundary condition to better capture practical scenarios. For the isotropic plate, the nonlinear eigenvalue approach with linear buckling gives an accurate post-buckling response up to $w_{\max}/h = 0.8$, which provides reasonable details about design and stability with smaller computational effort. Finally, the nonlinear buckling approach does not show any snapping behavior after $w_{\max}/h = 0.8$ unlike the nonlinear eigenvalue approach. It is shown in the next subsection that snapping is not observed in the post-buckling solution.

3.4.2. *Laminated plate with and without sinusoidal imperfection*

The effect of the geometric imperfection on the nonlinear buckling response is studied for both moderately thick and thin laminated composite plates using a symmetric cross-ply $(0°/90°/90°/0°)$ square laminated plate that is subjected to uniform uniaxial load with simply supported (SSSS) boundary condition and made of material MM1 [7]. The variation of the normalized load parameter $\bar{P} = Pb^2/h^3E_2$ with normalized deflection $\bar{w} = w_{\max}/h$ for different imperfection amplitude is plotted in Fig. 10 for the C^0 FEM-TSDT model via both nonlinear eigenvalue and nonlinear buckling approaches and for ANSYS solutions. Similarly, the through-thickness variation of stresses for both moderately thick and thin plates is plotted in Figs. 11 and 12, respectively, highlighting the importance of HSDT models over FSDT model.

The initial buckling strength of the plate with $a/h = 100$ using pre-buckling approach is 23.3927 (von Kármán) and 23.3927 (Green–Lagrange), while with linear buckling approach it is 24.4712 (von Kármán) and 24.4646 (Green–Lagrange). When $a/h = 10$, the initial buckling strength using pre-buckling approach is 14.1967 (von Kármán) and 13.9812 (Green–Lagrange), while with linear buckling it is 14.848 (von Kármán) and 14.6393 (Green–Lagrange). It is observed from Fig. 10 that the effect of nonlinearity is important for moderately-thick or thick plates as results obtained using Green–Lagrange nonlinearity are observed to be closer to ANSYS solutions and lower than those obtained using von Kármán nonlinearity. Further, the secondary path is well traced by the nonlinear buckling approach for both perfect and imperfect plates with moderate thickness. Also, the tertiary path for moderately thick plates with Green–Lagrange nonlinearity is well traced and without snapping.

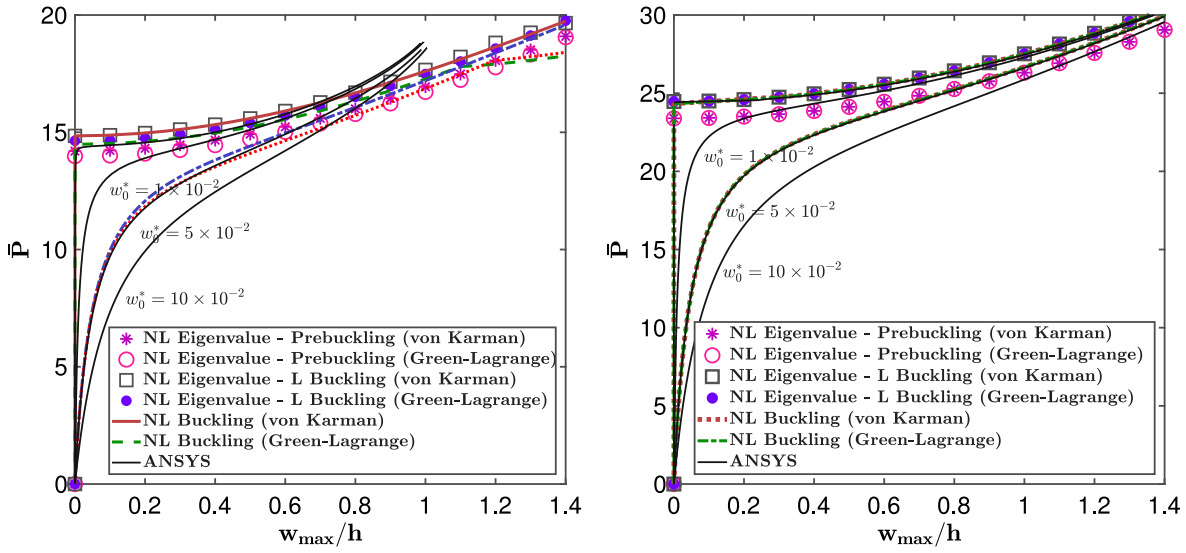

(a) $a/h = 10$. **(b)** $a/h = 100$.

Fig. 10. Buckling characteristic of simply supported (SSSS) square laminated (0°/90°/90°/0°) plate with and without imperfection under uniaxial loads.

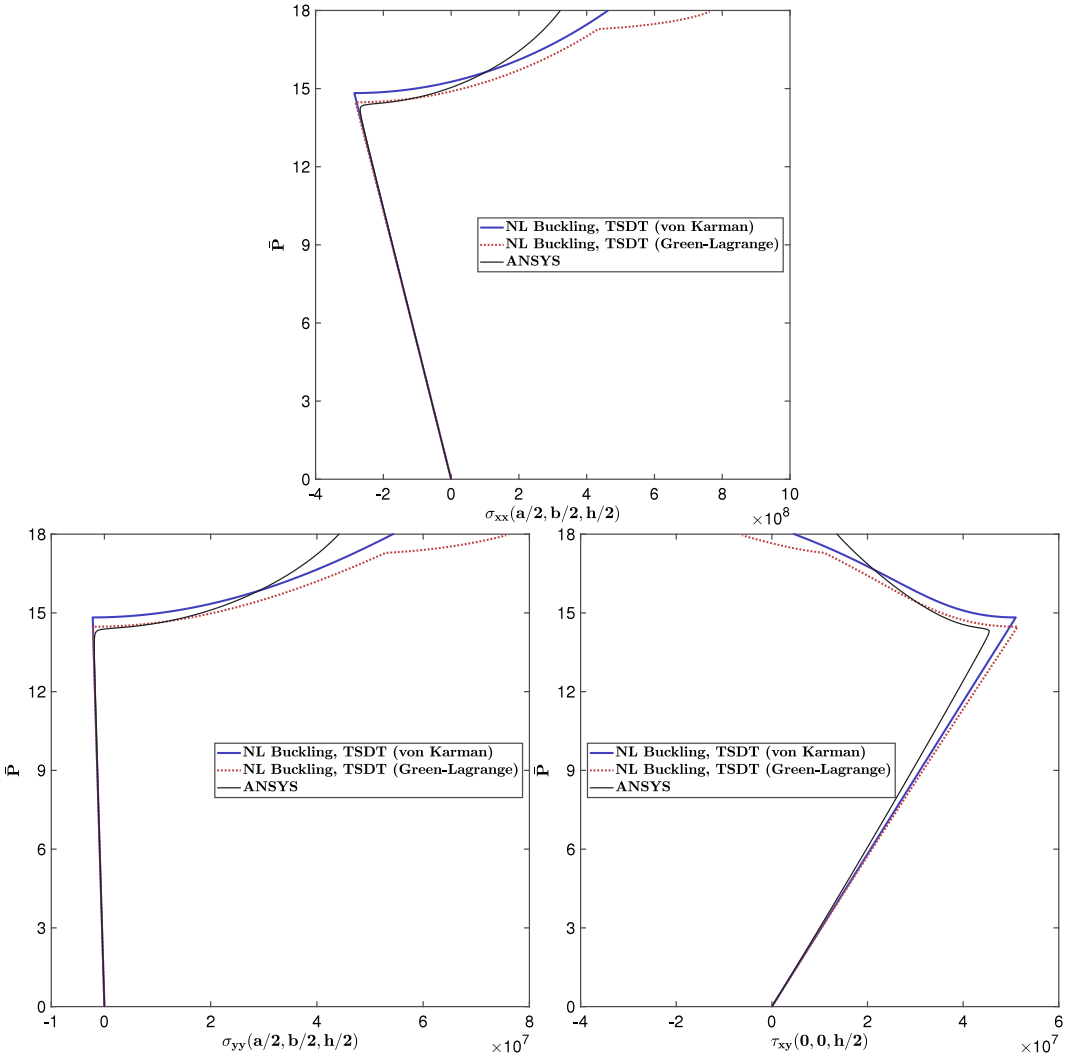

Fig. 11. Variation of stresses at critical points for buckling and post-buckling analysis of simply supported (SSSS) square laminated (0°/90°/90°/0°) plate without imperfection under uniaxial loads with $a/h = 10$.

Table 6
Normalized buckling load ($\bar{P} = Pb^2/E_2h^3$) of square laminated $(0°/90°)_s$ plate subjected to different uniaxial and biaxial compression with $b/h = 10$.

Boundary conditions	Approach	Uniform		Parabolic		Sinusoidal		Inverse sinusoidal		Triangular		Inverse triangular	
		Case-1	Case-2	Case-1	Case-2	Case-1	Case-2	Case-1	Case-2	Case-1	Case-2	Case-1	Case-2
CCCC	Pre-buckling[a]	41.6101	21.3875	46.7739	24.1825	47.6244	24.6185	106.671	65.3206	56.0883	28.9738	87.8949	53.3328
	Pre-buckling[b]	37.7173	21.1996	40.9670	23.9757	41.4359	24.4092	71.3699	64.2231	47.2408	28.7330	59.9920	52.6483
	ANSYS	39.5000	19.3110	44.5770	22.1470	45.3280	22.5690	53.7940	34.3760	48.9860	26.5810	50.6890	32.2850
FCCC	Pre-buckling[a]	34.0013	10.3551	45.1905	12.4010	46.1975	12.6717	55.3508	37.3886	54.8826	15.0447	47.9761	26.6403
	Pre-buckling[b]	33.6614	10.2322	40.9669	12.3095	41.4358	12.5824	51.5044	35.9077	47.2408	14.9485	46.9252	26.0109
	ANSYS	33.3710	9.6578	43.1980	11.6160	44.0560	11.8760	49.8770	11.3490	48.9860	14.0910	46.7360	23.4480
	Linear buckling[a]	–	11.8257	–	13.2422	–	13.4903	–	45.7773	–	15.9233	–	33.1296
	Linear buckling[b]	–	11.7963	–	13.2075	–	13.4546	–	45.5123	–	15.8789	–	33.0155
	ANSYS	–	10.9050	–	12.3210	–	12.5600	–	32.4470	–	14.8140	–	27.8020
CCCF	Pre-buckling[a]	18.7770	10.9138	20.4697	16.4376	20.8202	17.1274	70.5157	28.4292	24.4708	21.2169	53.3124	53.3124
	Pre-buckling[b]	18.6061	10.8373	20.3028	16.3218	20.6525	17.0063	69.3553	28.2250	24.2804	21.0635	52.7167	52.7167
	ANSYS	17.8320	10.1600	19.5790	15.3460	19.9240	16.0010	51.5970	21.3500	23.4050	19.8890	46.9260	19.9020
	Linear buckling[a]	18.6543	18.6543	20.6843	20.6843	21.0444	21.0444	67.3857	67.3857	24.7226	24.7226	51.9325	51.9325
	Linear buckling[b]	18.4895	18.4895	20.5185	20.5185	20.8776	20.8776	66.3255	66.3255	24.5332	24.5332	51.3669	51.3669
	ANSYS	17.7350	17.7350	19.7820	19.7820	20.1370	20.1370	51.3820	51.3820	23.6430	23.6430	46.2670	46.2670
CFFC	Pre-buckling[a]	7.8575	3.6030	12.5763	6.3980	13.1298	6.7573	15.1470	6.6827	16.4645	8.7110	12.4527	5.5177
	Pre-buckling[b]	7.8032	3.5854	12.4995	6.3700	13.0502	6.7281	15.0228	6.6457	16.3664	8.6746	12.3556	5.4883
	ANSYS	7.8037	3.5422	12.3980	6.2493	12.9270	6.5909	15.0850	6.5952	16.1470	8.4639	12.4070	5.4445
	Linear buckling[a]	7.8568	3.6018	12.4325	6.3462	13.0574	6.7025	15.3957	6.7808	16.3732	8.6585	12.5967	5.5758
	Linear buckling[b]	7.8027	3.5442	12.4325	6.3174	12.9787	6.6724	15.2709	6.7440	16.2765	8.6104	12.4995	5.5465
	ANSYS	7.8035	3.5412	12.3380	6.2023	12.8640	6.5417	15.3340	6.6906	16.0690	8.4088	12.5500	5.5011
CFCF	Pre-buckling[a]	12.5250	7.0167	13.6274	10.2183	13.8795	10.6281	66.9511	20.2504	16.4450	13.1875	43.1078	14.7409
	Pre-buckling[b]	12.4445	6.9687	13.5587	10.1566	13.8115	10.5653	45.1617	20.0764	16.3714	13.1148	40.1904	14.6182
	ANSYS	11.2100	6.3253	12.3200	9.2132	12.5590	9.5824	51.3750	18.2700	14.8940	11.8890	37.5650	13.2990
	Linear buckling[a]	12.3937	12.3937	13.8063	13.8063	14.0681	14.0681	63.4576	63.4576	16.6700	16.6700	40.9656	40.9656
	Linear buckling[b]	12.3157	12.3157	13.7369	13.7369	13.9995	13.9995	56.8150	56.8150	16.5956	16.5956	40.5648	40.5648
	ANSYS	11.1030	11.1030	12.4700	12.4700	12.7180	12.7180	50.7760	50.7760	15.0870	15.0870	35.9280	35.9280
FCFC	Pre-buckling[a]	33.2773	9.5918	42.7294	11.4123	43.7836	11.6620	53.0052	36.9358	52.4646	13.8676	45.7429	25.7897
	Pre-buckling[b]	33.1131	9.4759	40.9668	11.3262	41.4358	11.5780	51.5025	35.4987	47.2407	13.7775	44.7938	25.7897
	ANSYS	32.6720	9.0288	41.5360	10.8070	42.4750	11.0500	49.8770	29.5980	48.9860	13.1370	44.8710	22.8800
	Linear buckling[a]	–	11.0186	–	12.3553	–	12.5926	–	45.3978	–	14.9007	–	32.0036
	Linear buckling[b]	–	10.9944	–	12.3277	–	12.5643	–	45.1433	–	14.8662	–	31.9008
	ANSYS	–	10.2510	–	11.6080	–	11.8400	–	32.3810	–	14.0040	–	27.1790
CFFF	Pre-buckling[a]	1.1494	0.8779	1.9552	1.6217	2.0684	1.7294	2.4707	1.7158	2.6926	2.2932	1.9434	1.3839
	Pre-buckling[b]	1.1447	0.8743	1.9459	1.6136	2.0584	1.7206	2.4632	1.7107	2.6794	2.2811	1.9370	1.3794
	ANSYS	1.1055	0.8494	1.8699	1.5579	1.9758	1.6590	2.3953	1.6733	2.5645	2.1925	1.8819	1.3479
	Linear buckling[a]	1.1492	0.8777	1.9588	1.5987	2.0724	1.7026	2.4642	1.7403	2.6982	2.2512	1.9399	1.3984
	Linear buckling[b]	1.1444	0.8741	1.9495	1.5907	2.0624	1.6939	2.4568	1.7352	2.6849	2.2394	1.9335	1.3939
	ANSYS	1.1053	0.84924	1.8731	1.5362	1.9794	1.6337	2.3892	1.6971	2.5697	2.1531	1.8786	1.3620
FFFC	Pre-buckling[a]	6.2460	2.1695	8.9669	3.9731	9.3200	4.2288	12.9801	4.2027	11.6257	5.5762	10.9828	3.4068
	Pre-buckling[b]	6.2296	2.1592	8.9405	3.9531	9.2923	4.2075	12.8284	4.1847	11.5900	5.5481	10.8442	3.3918
	ANSYS	6.2409	2.1426	8.9648	3.9000	9.3139	4.1451	12.9710	4.1744	11.5920	5.4474	10.9690	3.3818
	Linear buckling[a]	6.2460	2.1692	8.9621	3.9242	9.3140	4.1724	13.5098	4.2568	11.6147	5.4907	11.3233	3.4388
	Linear buckling[b]	6.2296	2.1588	8.9360	3.9044	9.2865	4.1512	13.3486	4.2386	11.5795	5.4628	11.1779	3.4237
	ANSYS	6.2409	2.1423	8.9609	3.8541	9.3088	4.0924	13.4910	4.2267	11.5820	5.3680	11.3040	3.4129

Case-1 : uniaxial compression; Case-2 : biaxial compression.

[a] Present FEM-TSDT solution using von Kármán nonlinearity.

[b] Present FEM-TSDT solution using Green–Lagrange nonlinearity.

3.4.3. Simply supported anti-symmetric cross-ply laminated plate

In this numerical example, two simply supported (SSSS) square laminated $(0°/90°)_n$ plates with $a/h = 10$ and 100 and subjected to uniform uniaxial load are considered. The problem deals with nonlinear buckling analysis for which MM1 [47] with $E_1/E_2 = 40$ is used as material properties for all the layers (see Table 1). The same problem with $a/h = 100$ is studied by Giri and Simitses [47], and Prabhakara [46] using CLPT in conjunction with von Kármán nonlinearity. The plots of the normalized central deflection $w\left(\frac{a}{2}, \frac{b}{2}\right)/h$ against the normalized load parameter $\bar{P} = Pb^2/E_2h^3$ for $n = 1, 2, 5$, and 10 are shown in Fig. 13. It is observed that anti-symmetric cross-ply laminated plates do not exhibit bifurcation buckling due to the presence of bending-stretching coupling. Further, the linear buckling analysis and nonlinear eigenvalue approach for post-buckling analysis is not reliable for anti-symmetric plates because bifurcation is observed as in Sections 3.3.2 and 3.3.3. Hence, nonlinear analysis is preferred for a reliable and effective analysis of general composite plates under in-plane compression load. For the sake of completeness, the through-thickness variation of stresses for both moderately thick and thin plates is plotted in Figs. 14 and 15 which clearly show the need of HSDT model for the design and buckling analysis of composite plates.

3.4.4. Effect of aspect ratio on nonlinear buckling response

Following the extensive validation of the present nonlinear formulation, the effect of aspect ratio on post-buckling response of laminated composite plates is now investigated using the present C^0 FEM-TSDT model. A simply supported (SSSS) thin $(b/h = 100)$ rectangular laminated $(0°/90°/0°)$ plate with material properties MM2 [7] is considered. The plate is subjected to uniform uniaxial loads with magnitude P. The plots of the normalized deflection $w_{\max}/h$ against the normalized load $\hat{P} = \bar{P}/\bar{P}_{\text{critical}}$ for different aspect ratios $a/b =$

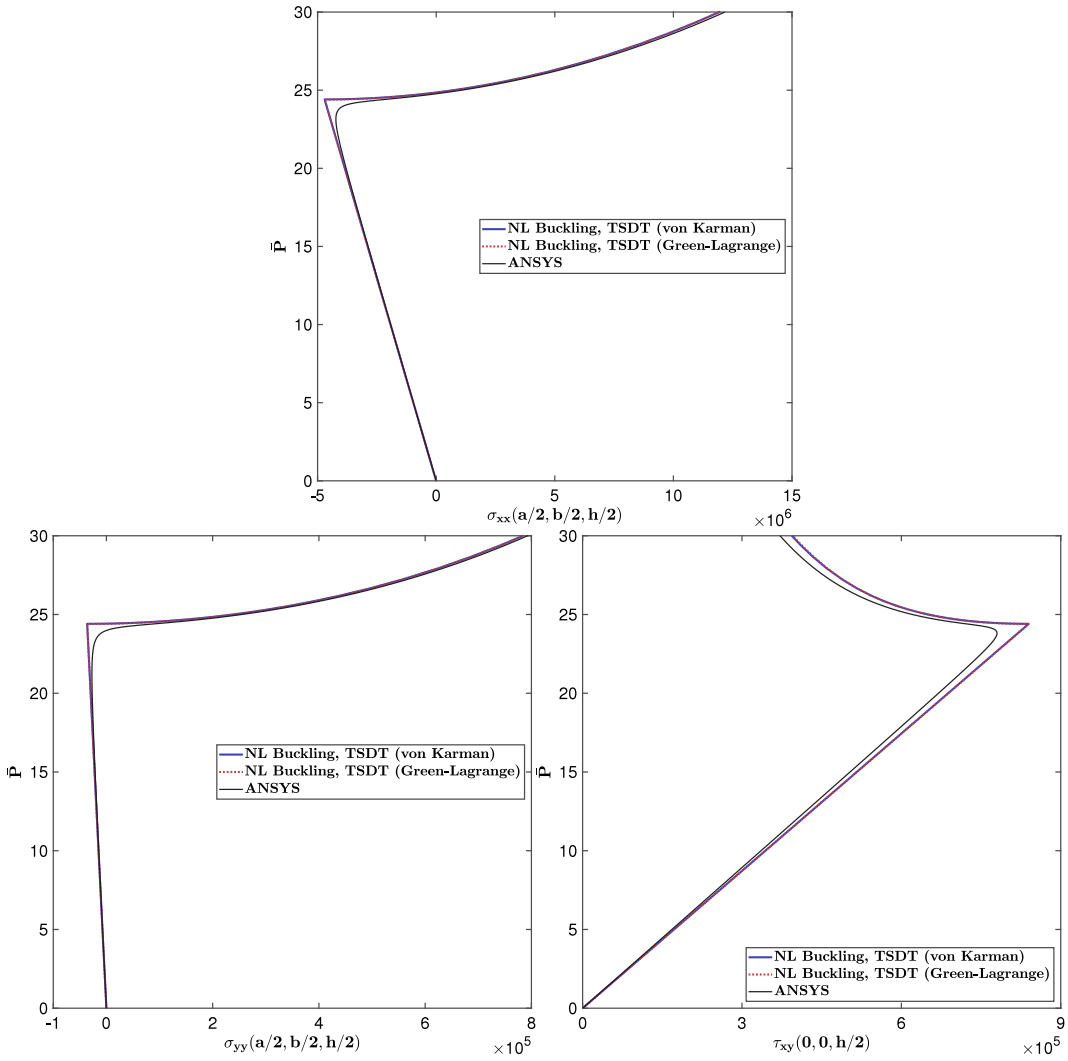

Fig. 12. Variation of stresses at critical points for buckling and post-buckling analysis of simply supported (SSSS) symmetric square laminated $(0°/90°/90°/0°)$ plate without imperfection under uniaxial loads with $a/h = 100$.

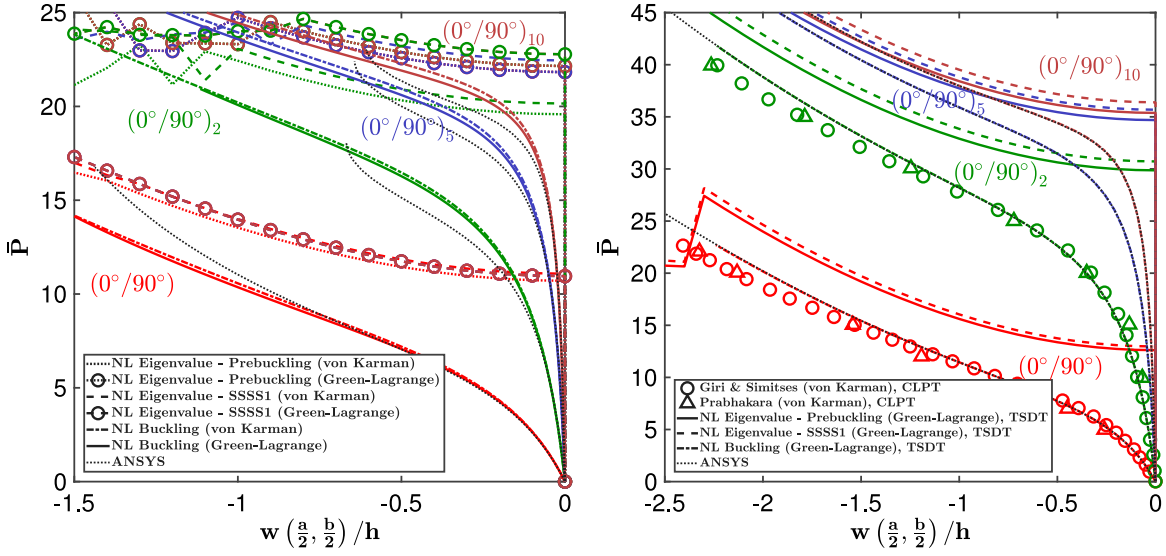

(a) $a/h = 10$. **(b)** $a/h = 100$.

Fig. 13. Nonlinear response of anti-symmetric cross-ply square laminated plate under uniaxial loads.

Table 7
Normalized buckling load ($\bar{P} = Pb^2/E_2h^3$) of square laminated $(0°/90°)_s$ plate subjected to different uniaxial and biaxial compression with $b/h = 10$.

Boundary conditions	Approach	Uniform		Parabolic		Sinusoidal		Inverse sinusoidal		Triangular		Inverse triangular	
		Case-1	Case-2	Case-1	Case-2	Case-1	Case-2	Case-1	Case-2	Case-1	Case-2	Case-1	Case-2
CCCS	Pre-buckling[a]	36.7508	18.2925	41.6735	21.0130	42.4877	21.4423	105.737	58.9499	50.3383	25.4704	87.1819	48.7560
	Pre-buckling[b]	36.3004	18.1294	40.9669	20.8396	41.4358	21.2671	71.3697	58.0270	47.2407	25.2695	59.9919	48.1535
	ANSYS	35.2060	17.1070	40.1670	19.7230	40.9710	20.1290	53.7930	34.3730	48.4950	23.8660	50.6890	32.2830
	Linear buckling[a]	37.6118	37.6118	42.8058	42.8058	43.7066	43.7066	116.004	116.004	52.0544	52.0544	94.0835	94.0835
	Linear buckling[b]	37.1662	37.1662	42.3307	42.3307	43.0765	43.0765	89.5160	89.5160	49.2066	49.2066	72.2545	72.2545
	ANSYS	36.1060	36.1060	41.3660	41.3660	42.2570	42.2570	59.3260	59.3260	49.7090	49.7090	55.5920	55.5920
SCCC	Pre-buckling[a]	39.6359	18.6368	45.6789	22.2724	46.5937	22.8528	101.002	61.3503	55.1239	27.6750	83.3492	48.7023
	Pre-buckling[b]	37.2953	18.4570	40.9669	22.0876	41.4358	22.6643	51.5398	53.8968	47.2408	27.4477	46.9416	47.8365
	ANSYS	38.0310	17.2460	43.5100	20.7900	44.3100	21.3490	53.7920	34.3730	48.9860	25.8840	50.5530	32.2830
	Linear buckling[a]	–	24.2574	–	27.7824	–	28.3948	–	78.3409	–	33.9489	–	63.7987
	Linear buckling[b]	–	24.1535	–	27.6621	–	28.2718	–	77.8937	–	33.8013	–	63.5105
	ANSYS	–	21.8080	–	25.1590	–	25.7220	–	38.9980	–	30.7020	–	36.2750
CSSC	Pre-buckling[a]	32.8153	15.7581	38.1634	18.7913	39.0162	19.2689	100.000	54.1805	46.6570	23.2738	82.7055	41.6980
	Pre-buckling[b]	32.3251	15.6059	37.7166	18.6457	38.5678	19.1220	51.5394	53.0225	46.1442	23.1026	46.9415	41.0600
	ANSYS	31.9770	14.9620	37.2810	17.9980	38.1160	18.4690	53.7920	34.3710	45.4810	22.3090	50.6880	32.2810
	Linear buckling[a]	34.6422	16.8703	40.0243	19.8981	40.9508	20.4219	110.937	58.0812	49.1395	24.7841	89.8260	45.5564
	Linear buckling[b]	34.1719	16.7247	39.5661	19.7485	40.4892	20.2700	77.0407	57.0072	48.6068	24.6044	65.8793	44.8930
	ANSYS	33.7520	16.0400	39.1430	19.0740	40.0550	19.5890	59.3300	37.9240	47.9880	23.7790	55.5960	35.0600
CSCS	Pre-buckling[a]	33.8477	15.3487	38.9503	17.7911	39.7787	18.1819	105.618	58.8757	47.4650	21.7271	87.0847	46.7565
	Pre-buckling[b]	33.4238	15.2141	38.5201	17.6492	39.3461	18.0386	71.3695	57.9746	46.9731	21.5625	59.9918	46.2178
	ANSYS	31.9590	14.5780	37.0160	16.9310	37.8310	17.3040	53.7930	34.3730	45.1600	20.6380	50.6890	32.2830
	Linear buckling[a]	33.6972	33.6972	38.2013	38.2013	39.0112	39.0112	113.801	113.801	46.5873	46.5873	92.0518	92.0518
	Linear buckling[b]	33.2869	33.2869	37.7866	38.2013	38.5938	38.5938	84.9529	84.9529	46.1113	46.1113	68.5186	68.5186
	ANSYS	31.8350	31.8350	36.3490	36.3490	37.1450	37.1450	59.1710	59.1710	44.3690	44.3690	55.5280	55.5280
SCSC	Pre-buckling[a]	37.0479	17.7940	43.2994	21.3363	44.2582	21.9062	100.981	61.3476	52.7722	26.6057	83.2414	48.692
	Pre-buckling[b]	36.4788	17.6169	40.9668	21.1487	41.4358	21.7142	51.5398	53.8968	47.2408	26.3700	46.9416	47.8201
	ANSYS	36.1540	16.5050	42.0130	19.9440	42.8720	20.4890	53.7920	34.3730	48.9860	24.8810	50.6880	32.2830
	Linear buckling[a]	–	22.6908	–	25.8246	–	26.3828	–	76.9341	–	31.5406	–	62.7722
	Linear buckling[b]	–	22.5994	–	25.7199	–	26.2758	–	76.5466	–	31.4125	–	62.5289
	ANSYS	–	20.8140	–	23.9440	–	24.4860	–	38.7690	–	29.3030	–	36.0650
SSSC	Pre-buckling[a]	29.4149	15.5823	34.5820	18.3518	35.4105	18.7963	99.9896	54.1467	42.5872	22.6328	82.6268	40.7609
	Pre-buckling[b]	28.9474	15.4385	34.1782	18.2231	35.0071	18.6672	51.5394	52.9905	42.1286	22.4846	46.9415	40.1674
	ANSYS	29.0120	14.8180	34.1960	17.9080	35.0160	18.3420	53.7920	34.3700	42.0230	22.0330	50.6880	32.2810
	Linear buckling[a]	31.2632	16.4327	36.4796	19.0866	37.3801	19.5530	110.880	57.6390	45.1024	23.5936	89.2904	44.2799
	Linear buckling[b]	30.8220	16.3018	36.0627	18.9588	36.9612	19.4240	77.0387	56.6285	44.6203	23.4432	65.8764	43.6867
	ANSYS	30.8340	15.5920	36.0890	18.5330	36.9820	19.0320	59.3450	37.9840	44.5400	22.9750	55.6080	35.2320
CSSS	Pre-buckling[a]	27.6970	12.7357	32.5093	15.1237	33.2809	15.5072	99.7753	54.1502	40.0231	18.7450	82.4624	36.8403
	Pre-buckling[b]	27.2786	12.6160	32.1334	15.0107	32.9051	15.3936	51.5390	52.9941	39.5979	18.6136	46.9414	36.3227
	ANSYS	26.8720	12.3600	31.6460	14.7460	32.4070	15.1240	53.7920	34.3700	38.9360	18.2610	50.6880	32.2810
	Linear buckling[a]	28.6715	13.4135	32.9169	15.6975	33.6734	16.0982	108.995	57.7426	40.4580	19.4964	88.1247	40.0309
	Linear buckling[b]	28.2609	13.2939	32.5393	15.5809	33.2957	15.9806	74.4939	56.6931	40.0300	19.3595	63.4497	39.4957
	ANSYS	27.8050	13.0210	32.0570	15.3210	32.8030	15.7170	59.1740	38.1960	39.3740	19.0170	55.5310	35.4040

Case-1 : uniaxial compression; Case-2 : biaxial compression.

[a] Present FEM-TSDT solution using von Kármán nonlinearity.

[b] Present FEM-TSDT solution using Green–Lagrange nonlinearity.

0.5, 1, 1.5, 2, 2.5, 3, 3.5, 4, 4.5, and 5 is depicted in Fig. 16. The results are obtained using both nonlinear eigenvalue and nonlinear buckling approaches for C^0 FEM-TSDT model in conjunction with von Kármán nonlinearity only (because of the thinness of the plate $b/h = 100$). The initial buckling strength $\bar{P}_{\text{critical}} = P_{\text{critical}}b^2/E_2h^3$ of the plates with the different aspect ratios $a/b = 0.5, 1, 1.5, 2, 2.5, 3, 3.5, 4, 4.5,$ and 5 are 126.4560, 35.9256, 20.9794, 18.3582, 20.0377, 20.9908, 18.8983, 18.3621, 18.8374, and 19.4187, respectively. It is observed from Fig. 16 that the plate buckling mode increases with increasing aspect ratio. The eigenvalue approach is accurate up to $w_{\max}/h = 0.5$ beyond which the nonlinear buckling approach must be used. The mode shapes shown in Fig. 16 are from the nonlinear buckling approach.

3.4.5. Effect of boundary conditions on nonlinear buckling response

At this juncture, the post-buckling response of laminated composite plates for different boundary condition, as done in the linear analysis, is examined using the present C^0 FEM-TSDT model for a thin $(b/h = 100)$ square laminated $(0°/90°/90°/0°)$ plate with material properties MM2 [7]. The plate is subjected to uniform uniaxial loads with magnitude P. The plots of the normalized deflection $w_{\max}/h$ against the normalized load $\hat{P} = \bar{P}/\bar{P}_{\text{critical}}$ for different set of boundary conditions are depicted in Fig. 17. The initial buckling strength $\bar{P}_{\text{critical}} = P_{\text{critical}}b^2/E_2h^3$ for different boundary conditions SSSS, SSSF, FSSS, SFSF, CCCF, CFCF, CFFC, and CFFF is 37.1875, 14.6629, 29.2266, 5.7219, 34.0197, 21.5856, 9.1742, and 1.3302, respectively. Fig. 17 indicates that the boundary condition has significant influence on buckling modes and their maximum deflection. Compared to the nonlinear eigenvalue with prebuckling approach, the nonlinear eigenvalue with linear buckling approach accurately captures the post-buckling response under different boundary conditions. The mode shapes shown in Fig. 17 are obtained using the nonlinear buckling approach.

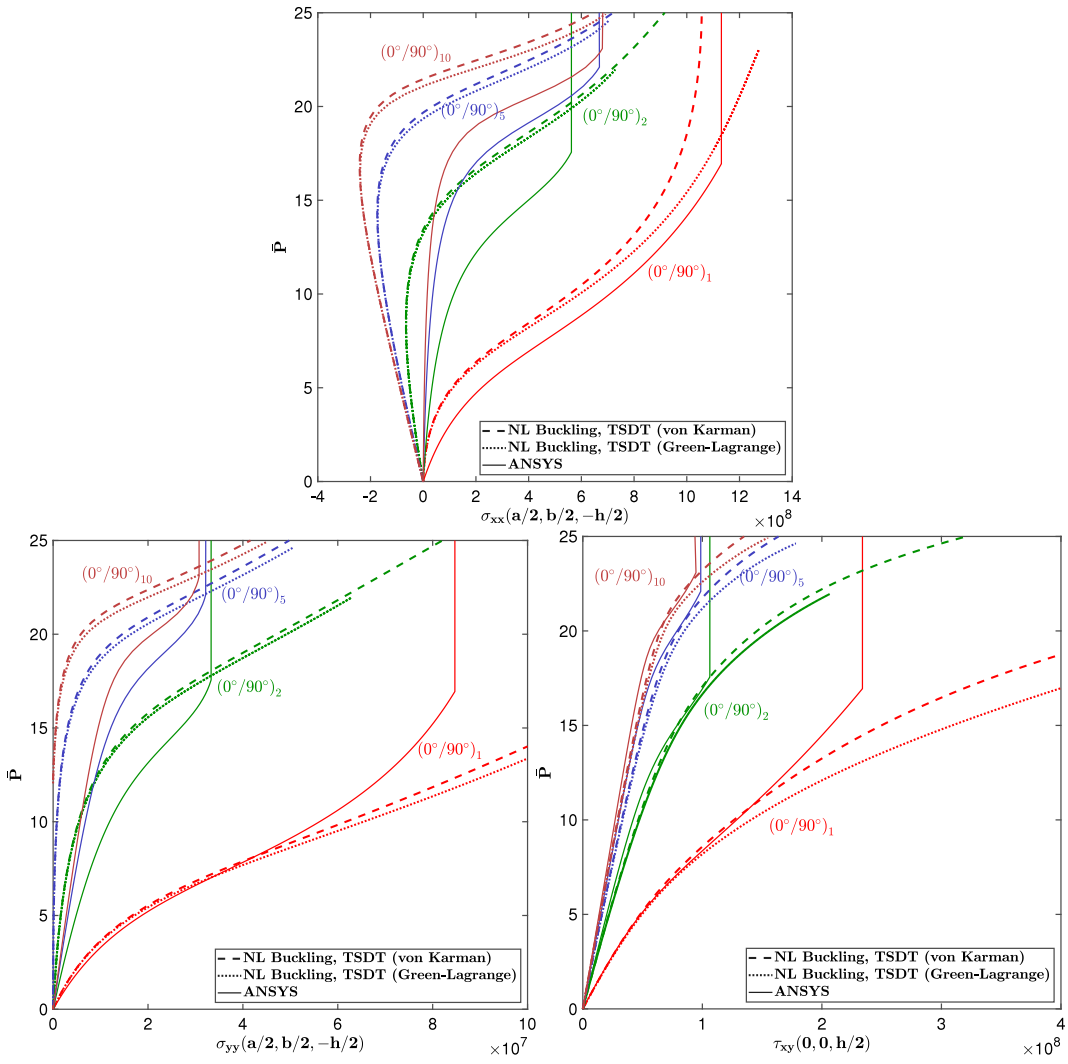

Fig. 14. Variation of stresses at critical points for buckling and post-buckling analysis of anti-symmetric cross-ply square laminated plates under uniaxial loads with $a/h = 10$.

3.4.6. Effect of fiber orientation on nonlinear buckling response

To investigate the influence of fiber orientation on post-buckling characteristics, a simply supported (SSSS) square angle-ply $(\theta/-\theta)$ laminated plate is employed. The geometric and material properties, and the in-plane loading used are the same as those specified in the preceding subsection, Section 3.4.5. Fig. 18 depicts the plots of the normalized deflection $w_{\max}/h$ against the normalized load $\hat{P} = \bar{P}/\bar{P}_{\text{critical}}$ for different ply orientation, and it is observed that angle-ply composite plates do not exhibit pure bifurcation. They first blend and then follow the secondary path. Further, post-buckling deflection profile depends upon fiber orientation as plates with lay-ups $(45°/-45°)$, $(60°/-60°)$, and $(75°/-75°)$ buckle with second buckling mode. The initial buckling strength $\bar{P}_{\text{critical}} = P_{\text{critical}} b^2/E_2 h^3$ obtained using linear buckling approach for the following lamination lay-up $(15°/-15°)$, $(30°/-30°)$, $(45°/-45°)$, $(60°/-60°)$ and $(75°/-75°)$ is 26.5240, 19.7367, 33.0916, 41.5325, and 26.8976, respectively. It is evident from Fig. 18 that the actual buckling load for angle-ply laminated is different from the value predicted by linear buckling approach. The mode shapes shown in the figure are obtained using the nonlinear buckling approach.

3.4.7. Effect of different types of imperfection on nonlinear buckling response

Generally, imperfection in a plate structure is either local or global and its nature or characterstic may affect post-buckling response of the plate. The initial deflection due to ang imperfection is modeled as a product of trigonometric and hyperbolic functions [15,17,39] and is expressed as

$$w^* = w_0^* h sech\left(\delta_1\left(\frac{x}{a} - \phi_1\right)\right) cos\left(\mu_1\left(\frac{x}{a} - \phi_1\right)\right) sech\left(\delta_2\left(\frac{y}{b} - \phi_2\right)\right) \times cos\left(\mu_2\left(\frac{y}{b} - \phi_2\right)\right)$$

Different types of imperfections are obtained as follows: Sine-type $\delta_1 = \delta_2 = 0$, $\mu_1 = \mu_2 = 1$, $\phi_1 = \phi_2 = 0.5$; Global-type: G1 $\delta_1 = \delta_2 = 0$, $\mu_1 = \mu_2 = 3$, $\phi_1 = \phi_2 = 0.5$; G2 $\delta_1 = \delta_2 = 0$, $\mu_1 = \mu_2 = 5$, $\phi_1 = \phi_2 = 0.5$; G3 $\delta_1 = \delta_2 = 0$, $\mu_1 = \mu_2 = 7$, $\phi_1 = \phi_2 = 0.5$; Local-type: L1 $\delta_1 = 15$, $\delta_2 = 0$, $\mu_1 = 2$, $\mu_2 = 1$, $\phi_1 = 0.25$, $\phi_2 = 0.5$; L2 $\delta_1 = 15$, $\delta_2 = 0$, $\mu_1 = 2$, $\mu_2 = 1$, $\phi_1 = 0.5$, $\phi_2 = 0.5$; L3 $\delta_1 = 15$, $\delta_2 = 0$, $\mu_1 = 2$, $\mu_2 = 3$, $\phi_1 = 0.5$, $\phi_2 = 0.5$; L4 $\delta_1 = 15$, $\delta_2 = 0$, $\mu_1 = 2$, $\mu_2 = 5$, $\phi_1 = 0.5$, $\phi_2 = 0.5$. The illustration of the different types of imperfection is shown in Fig. 19.

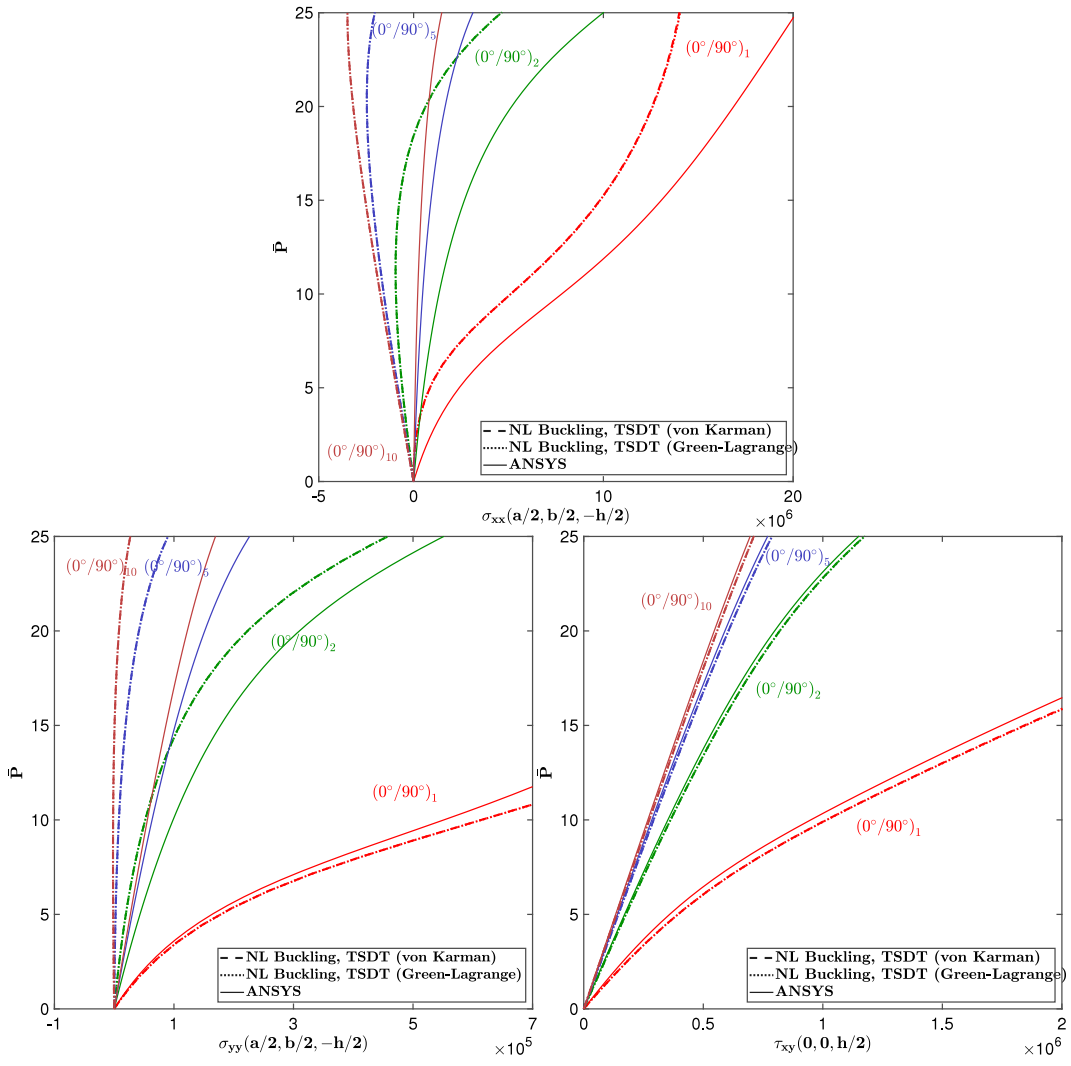

Fig. 15. Variation of stresses at critical points for buckling and post-buckling analysis of anti-symmetric cross-ply square laminated plates under uniaxial loads with $a/h = 100$.

The effect of the different types of imperfection is studied for a simply supported (SSSS) square laminated $(0°/90°/90°/0°)$ plate whose geometric and material properties and in-plane loading are identical to those specified in Section 3.4.5. The amplitude of imperfection is $w_0^* = 10^{-1}$. The normalized deflection $w_{\max}/h$ is plotted against the normalized load $\hat{P} = \bar{P}/\bar{P}_{\text{critical}}$ for different ply orientation as depicted in Fig. 20. The results show that post-buckling response is sensitive to the type of imperfection. The initial buckling strength $\bar{P}_{\text{critical}} = P_{\text{critical}} b^2/E_2 h^3$ obtained with the linear buckling approach for a perfect flat plate is 24.3991.

4. Conclusion

A comprehensive study to determine the reliability and suitability of different approaches for buckling analysis of multilayered composite plates under in-plane mechanical loads using a penalty based C^0 FEM-HSDT plate model with both von Kármán and Green–Lagrange nonlinearities is presented in this paper.

Regarding stress stiffening effect, Green–Lagrange nonlinearity formulation includes the contribution of in-plane displacement and predicts reliable and accurate buckling loads. A significant difference (ranging from 3% to 30%) is observed between the results obtained using von Kármán and those that employ Green–Lagrange stress stiffening for moderately thick plates. Thus, it is suggested to incorporate the Green–Lagrange nonlinearity in formulations for better design and stability analysis of moderately thick composite plates. It is also suggested to use consistent boundary conditions in pre-buckling and eigenvalue analysis as done in linear buckling approach for realistic predictions of buckling loads which can be verified from nonlinear buckling approach. Linear buckling analysis is observed to be reliable for only symmetric cross-ply laminated plates.

The nonlinear buckling approach is superior to the nonlinear eigenvalue approach. The nonlinear eigenvalue approach can be used for symmetric cross-ply laminated plate for $w_{\max}/h < 0.5$, else the nonlinear buckling approach is recommended. While the angle-ply laminated composite plates do not exhibit pure bifurcation, i.e, bending-buckling response, and a stable tertiary buckling path is also observed in some plate problems.

The proposed FEM-HSDT based unified formulation can be easily reduced to any particular HSDT by a simple selection of the particular transverse shear function, $f(z)$ with appropriate boundary conditions .

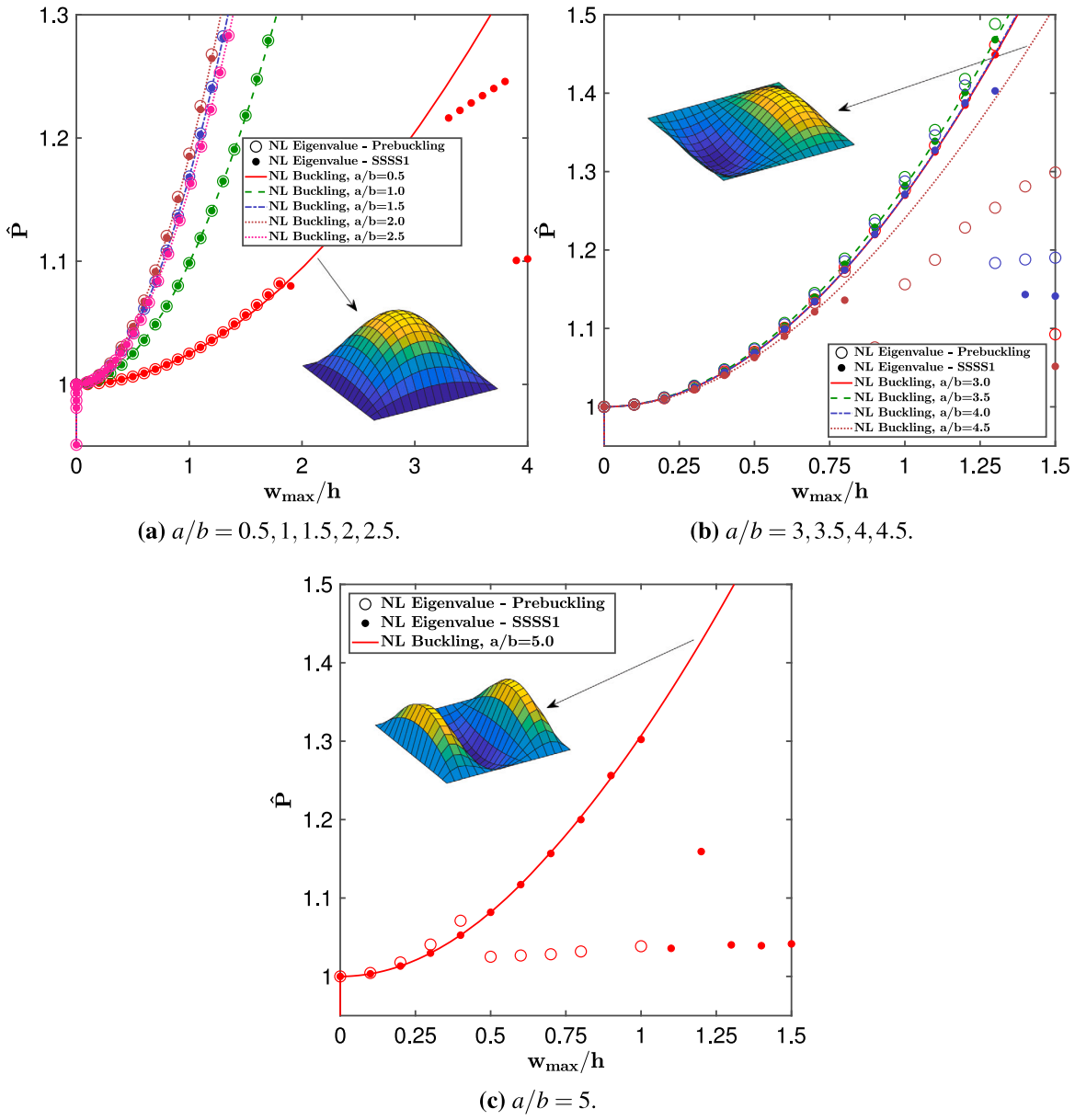

(a) $a/b = 0.5, 1, 1.5, 2, 2.5.$ **(b)** $a/b = 3, 3.5, 4, 4.5.$

(c) $a/b = 5.$

Fig. 16. Effect of aspect ratio (a/b) on post-buckling characteristics of simply supported (SSSS) laminated $(0°/90°/0°)$ rectangular plate under uniaxial loads with $b/h = 100$. The modes are obtained using the nonlinear buckling approach.

It is observed that the accuracy of IHSDT is limited to some particular laminated plates. Compared to IHSDT model, the TSDT and IHTSDT models are reliable for the determination of buckling characteristics and they predict approximately identical solutions. In other words, IHTSDT can be interpreted as an equivalent non-polynomial theory of TSDT. Unlike bending analysis, buckling analysis requires a very large penalty parameter γ, 10^3 times the Young's modulus. A common value of 10^3 times the Young's modulus can be utilized for both bending and buckling analysis of composite plates. Further, neglecting the contribution of penalty stiffness matrix leads to a lower buckling load, and the effect of the penalty parameter must be included in C^0 FE formulation for a solution that satisfies the characteristics of C^1 HSDT. Finally, the present model is suitable for buckling analysis of any general multilayered composite plate because it is systematically derived without presumption of uniform stress distribution.

CRediT authorship contribution statement

Surendra Verma: Conceptualization, Data curation, Methodology, Software, Visualization, Writing – original draft. **Abha Gupta:** Software, Visualization. **Babu Ranjan Thakur:** Software, Visualization. **Donatus Oguamanam:** Conceptualization, Methodology, Supervision, Writing – review & editing. **B.N. Singh:** Conceptualization, Methodology, Supervision.

Declaration of competing interest

The authors declare that they have no known competing financial interests or personal relationships that could have appeared to influence the work reported in this paper.

Data availability

Data will be made available on request.

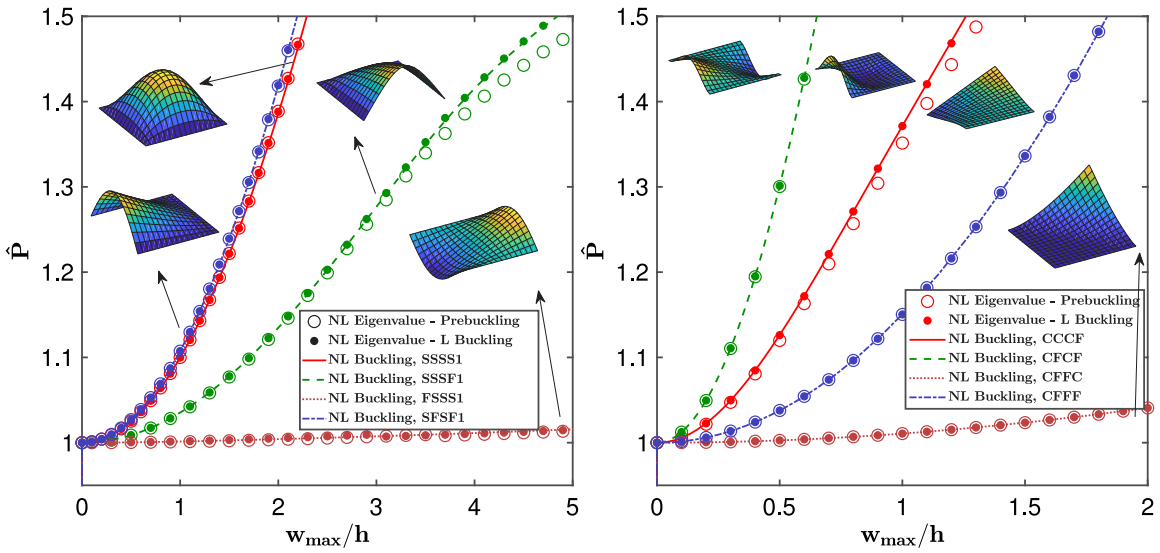

(a) SSSS, SSSF, FSSS, SFSF. **(b)** CCCF, CFCF, CFFC, CFFF.

Fig. 17. Effect of boundary condition on post-buckling characteristics of square laminated $(0°/90°/90°/0°)$ plate under uniaxial loads. The modes are obtained using the nonlinear buckling approach.

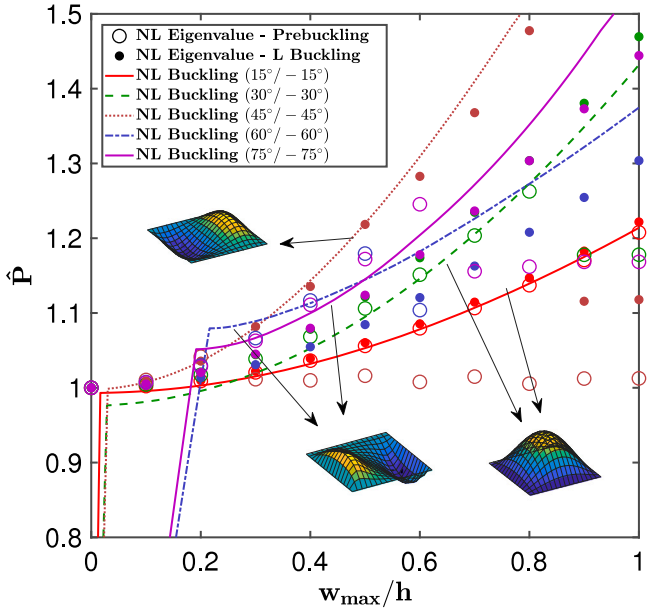

Fig. 18. Effect of fiber orientation on post-buckling characteristics of simply supported (SSSS) square laminated $(\theta°/-\theta°)$ plate under uniaxial loads. The modes are obtained using the nonlinear buckling approach.

Appendix. Navier solution for simply supported anti-symmetric cross-ply composite plate under in-plane mechanical loads

$$u_0 = \sum_{m=1}^{\infty}\sum_{n=1}^{\infty} U_{mn} cos(\alpha x)\, sin(\beta y) \qquad v_0 = \sum_{m=1}^{\infty}\sum_{n=1}^{\infty} V_{mn} sin(\alpha x)\, cos(\beta y)$$

$$w_0 = \sum_{m=1}^{\infty}\sum_{n=1}^{\infty} W_{mn} sin(\alpha x)\, sin(\beta y) \qquad \theta_x = \sum_{m=1}^{\infty}\sum_{n=1}^{\infty} X_{mn} cos(\alpha x)\, sin(\beta y)$$

$$\theta_y = \sum_{m=1}^{\infty}\sum_{n=1}^{\infty} Y_{mn} sin(\alpha x)\, cos(\beta y)$$

$$\left(\begin{bmatrix} K_{11} & K_{12} & K_{13} & K_{14} & K_{15} \\ & K_{22} & K_{23} & K_{24} & K_{25} \\ & & K_{33} & K_{34} & K_{35} \\ & \text{sym} & & K_{44} & K_{45} \\ & & & & K_{55} \end{bmatrix} - \lambda \begin{bmatrix} 0 & 0 & 0 & 0 & 0 \\ & 0 & 0 & 0 & 0 \\ & & K^{g}_{33} & 0 & 0 \\ & \text{sym} & & 0 & 0 \\ & & & & 0 \end{bmatrix}\right) \begin{Bmatrix} U_{mn} \\ V_{mn} \\ W_{mn} \\ X_{mn} \\ Y_{mn} \end{Bmatrix} = \begin{Bmatrix} 0 \\ 0 \\ 0 \\ 0 \\ 0 \end{Bmatrix}$$

$$K_{11} = \alpha^2 A_{11} + \beta^2 A_{66} \qquad K_{12} = \alpha\beta A_{12} + \alpha\beta A_{66}$$

$$K_{13} = -\alpha\left(\alpha^2 B_{11} + \beta^2 B_{12} + 2\beta^2 B_{66}\right) \qquad K_{14} = \alpha^2 C_{11} + \beta^2 C_{66}$$

$$K_{15} = \alpha\beta C_{12} + \alpha\beta C_{66} \qquad K_{22} = \alpha^2 A_{66} + \beta^2 A_{22}$$

$$K_{23} = -\beta\left(\alpha^2 B_{12} + \beta^2 B_{22} + 2\alpha^2 B_{66}\right) \qquad K_{24} = \alpha\beta C_{12} + \alpha\beta C_{66}$$

$$K_{25} = \alpha^2 C_{66} + \beta^2 C_{22} \qquad K_{33} = \alpha^4 D_{11} + 2\alpha^2\beta^2 D_{12} + \beta^4 D_{22} + 4\alpha^2\beta^2 D_{66}$$

$$K_{34} = -\alpha\left(\alpha^2 E_{11} + \beta^2 E_{12} + 2\beta^2 E_{66}\right) \qquad K_{35} = -\beta\left(\alpha^2 E_{12} + \beta^2 E_{22} + 2\alpha^2 E_{66}\right)$$

$$K_{44} = A_{55} + \alpha^2 F_{11} + \beta^2 F_{66} \qquad K_{45} = \alpha\beta F_{12} + \alpha\beta F_{66}$$

$$K_{55} = A_{44} + \alpha^2 F_{66} + \beta^2 F_{22} \qquad K^{g}_{33} = K^{gm}_{33}$$

$K^{gm}_{33} = \alpha^2$ Uniaxial uniform loading in x-direction

$K^{gm}_{33} = \beta^2$ Uniaxial uniform loading in y-direction

$K^{gm}_{33} = \alpha^2 + \left(N_y/N_x\right)\beta^2$ Biaxial uniform loading in both directions

$$\left[A_{ij}\right] = \int_{-h/2}^{h/2} f'(z)\,\bar{Q}_{ij}\,dz \qquad i,j = 4,5$$

$$\left[A_{ij}\right] = \int_{-h/2}^{h/2} \bar{Q}_{ij}\,dz \qquad \left[B_{ij}\right] = \int_{-h/2}^{h/2} z\bar{Q}_{ij}\,dz \qquad \left[C_{ij}\right] = \int_{-h/2}^{h/2} f(z)\,\bar{Q}_{ij}\,dz$$

$$\left[D_{ij}\right] = \int_{-h/2}^{h/2} G(z)\,\bar{Q}_{ij}\,dz \qquad \left[E_{ij}\right] = \int_{-h/2}^{h/2} z^2\bar{Q}_{ij}\,dz \qquad \left[F_{ij}\right] = \int_{-h/2}^{h/2} z f(z)\,\bar{Q}_{ij}\,dz$$

$$i,j = 1,2,6$$

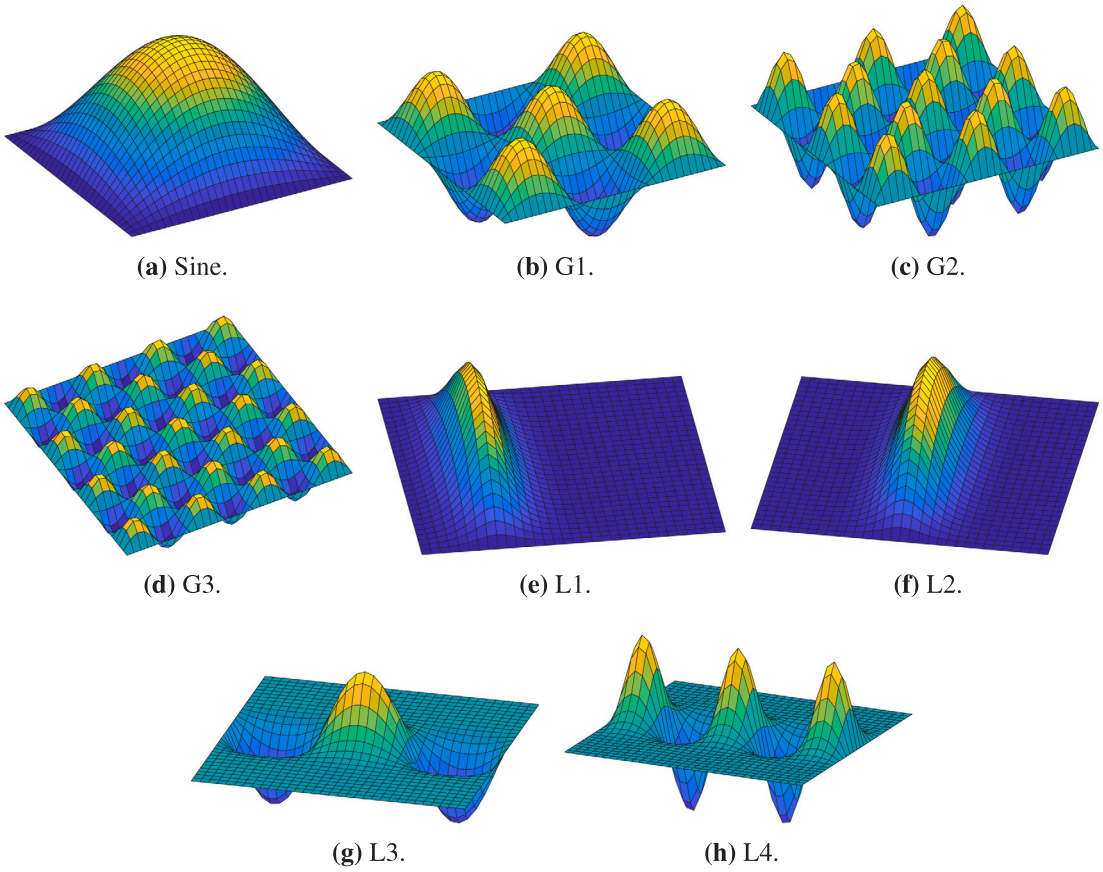

Fig. 19. Different types of imperfection.

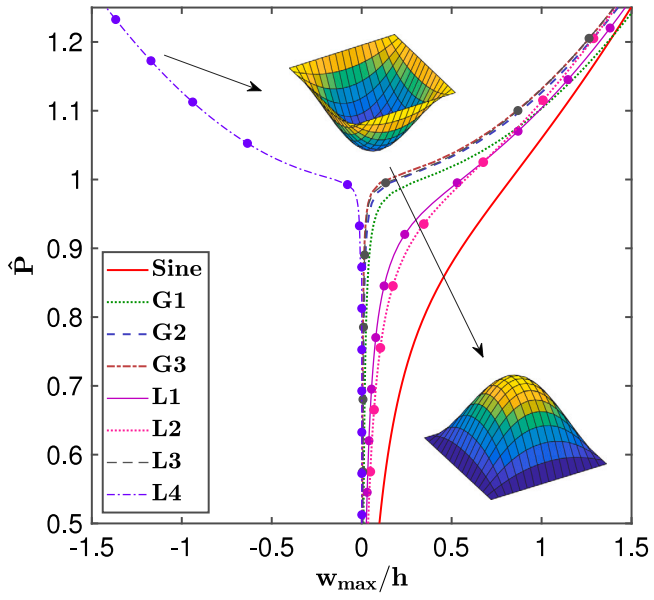

Fig. 20. Effect of different types of imperfection on post-buckling characteristics of simply supported (SSSS) square laminated (0°/90°/90°/0°) plate under uniaxial loads.

Lowest buckling load (λ) is obtained by considering Navier solution for $m = n = 1$.

References

[1] A. Garg, M. Belarbi, H. Chalak, L. Li, A. Sharma, M. Avcar, N. Sharma, S. Paruthi, R. Gulia, Buckling and free vibration analysis of bio-inspired laminated sandwich plates with helicoidal/Bouligand face sheets containing softcore, Ocean Eng. 270 (2023) 113684, http://dx.doi.org/10.1016/j.oceaneng.2023.113684.

[2] K. Zahari, Y. Hilali, S. Mesmoudi, R.E. khaoulani, O. Bourihane, Review and comparison of thin and thick FGM plate theories using a unified buckling formulation, Structures 46 (2022) 1545–1560, http://dx.doi.org/10.1016/j.istruc.2022.10.115.

[3] A. Maji, P.K. Mahato, Development and applications of shear deformation theories for laminated composite plates: An overview, J. Thermoplast. Compos. Mater. 35 (12) (2020) 2576–2619, http://dx.doi.org/10.1177/0892705720930765.

[4] R. Sahoo, B.N. Singh, Assessment of inverse hyperbolic zigzag theory for buckling analysis of laminated composite and sandwich plates using finite element method, Arch. Appl. Mech. 91 (1) (2020) 169–186, http://dx.doi.org/10.1007/s00419-020-01761-9.

[5] X. Xu, E. Carrera, H. Yang, E. Daneshkhah, R. Augello, Evaluation of stiffeners effects on buckling and post-buckling of laminated panels, Aerosp. Sci. Technol. 123 (2022) 107431, http://dx.doi.org/10.1016/j.ast.2022.107431.

[6] S. Abrate, M.D. Sciuva, Equivalent single layer theories for composite and sandwich structures: A review, Compos. Struct. 179 (2017) 482–494, http://dx.doi.org/10.1016/j.compstruct.2017.07.090.

[7] J.N. Reddy, Mechanics of Laminated Composite Plates and Shells, CRC Press, 2004, http://dx.doi.org/10.1201/b12409.

[8] S. Verma, B.R. Thakur, B. Singh, D. Maiti, Geometrically nonlinear flexural analysis of multilayered composite plate using polynomial and non-polynomial shear deformation theories, Aerosp. Sci. Technol. 112 (2021) 106635, http://dx.doi.org/10.1016/j.ast.2021.106635.

[9] S.T. Dennis, A.N. Palazotto, The effect of non-linear curvature strains on the buckling of laminated plates and shells, Internat. J. Numer. Methods Engrg. 36 (4) (1993) 595–609, http://dx.doi.org/10.1002/nme.1620360404.

[10] G. Singh, G. Rao, N. Iyengar, Bifurcation buckling of unsymmetrically laminated plates, Compos. Eng. 4 (2) (1994) 181–194, http://dx.doi.org/10.1016/0961-9526(94)90026-4.

[11] P. Sundaresan, G. Singh, G. Rao, Buckling and post-buckling analysis of moderately thick laminated rectangular plates, Comput. Struct. 61 (1) (1996) 79–86, http://dx.doi.org/10.1016/0045-7949(96)00010-7.

[12] E. Ruocco, V. Mallardo, Buckling analysis of levy-type orthotropic stiffened plate and shell based on different strain-displacement models, Int. J. Non-Linear Mech. 50 (2013) 40–47, http://dx.doi.org/10.1016/j.ijnonlinmec.2012.11.007.

[13] E. Ruocco, V. Minutolo, Buckling analysis of mindlin plates under the Green–Lagrange strain hypothesis, Int. J. Struct. Stab. Dyn. 15 (06) (2015) 1450079, http://dx.doi.org/10.1142/s0219455414500795.

[14] N. Sharma, M. Nishad, D.K. Maiti, M.R. Sunny, B.N. Singh, Uncertainty quantification in buckling strength of variable stiffness laminated composite plate under thermal loading, Compos. Struct. 275 (2021) 114486, http://dx.doi.org/10.1016/j.compstruct.2021.114486.

[15] M. Cetkovic, Influence of initial geometrical imperfections on thermal stability of laminated composite plates using layerwise finite element, Compos. Struct. 291 (2022) 115547, http://dx.doi.org/10.1016/j.compstruct.2022.115547.

[16] T. Le-Manh, J. Lee, Postbuckling of laminated composite plates using NURBS-based isogeometric analysis, Compos. Struct. 109 (2014) 286–293, http://dx.doi.org/10.1016/j.compstruct.2013.11.011.

[17] L.V. Tran, S.-E. Kim, Stability analysis of multi-layered plates subjected to partial edge compression with and without initial imperfection, Compos. Struct. 205 (2018) 26–41, http://dx.doi.org/10.1016/j.compstruct.2018.08.065.

[18] C.D. Kalfountzos, G.S. Bikakis, E.E. Theotokoglou, Postbuckling and secondary buckling of rectangular fiber-metal laminates and glass-fiber reinforced composites under uniaxial compression, Eng. Struct. 267 (2022) 114663, http://dx.doi.org/10.1016/j.engstruct.2022.114663.

[19] I. Shufrin, M. Eisenberger, Stability of variable thickness shear deformable plates—first order and high order analyses, Thin-Walled Struct. 43 (2) (2005) 189–207, http://dx.doi.org/10.1016/j.tws.2004.07.013.

[20] A. Chakrabarti, A.H. Sheikh, Buckling of laminated sandwich plates subjected to partial edge compression, Int. J. Mech. Sci. 47 (3) (2005) 418–436, http://dx.doi.org/10.1016/j.ijmecsci.2005.01.005.

[21] A. Chakrabarti, A.H. Sheikh, Buckling of composite laminates subjected to in-plane partial edge compression using a refined plate theory, J. Reinf. Plast. Compos. 25 (11) (2006) 1189–1204, http://dx.doi.org/10.1177/0731684406066368.

[22] T. Rajanna, S. Banerjee, Y.M. Desai, D. Prabhakara, Effect of boundary conditions and non-uniform edge loads on buckling characteristics of laminated composite panels with and without cutout, Int. J. Comput. Methods Eng. Sci. Mech. 18 (1) (2017) 64–76, http://dx.doi.org/10.1080/15502287.2016.1276350.

[23] T. Rajanna, S. Banerjee, Y.M. Desai, D.L. Prabhakara, Effect of reinforced cutouts and ply-orientations on buckling behavior of composite panels subjected to non-uniform edge loads, Int. J. Struct. Stab. Dyn. 18 (04) (2018) 1850058, http://dx.doi.org/10.1142/s021945541850058x.

[24] B. Adhikari, B.N. Singh, Buckling characteristics of laminated functionally-graded CNT-reinforced composite plate under nonuniform uniaxial and biaxial in-plane edge loads, Int. J. Struct. Stab. Dyn. 20 (02) (2019) 2050022, http://dx.doi.org/10.1142/s0219455420500224.

[25] S.N. Patel, A.H. Sheikh, Buckling response of laminated composite stiffened plates subjected to partial in-plane edge loading, Int. J. Comput. Methods Eng. Sci. Mech. 17 (5–6) (2016) 322–338, http://dx.doi.org/10.1080/15502287.2016.1231235.

[26] S.J. Nima, R. Ganesan, Buckling analysis of symmetrically laminated composite plates including the effect of variable pre-stress field using the Ritz method, Eur. J. Mech. A Solids 90 (2021) 104323, http://dx.doi.org/10.1016/j.euromechsol.2021.104323.

[27] K. Prajapat, S. Ray-Chaudhuri, A. Kumar, Effect of in-plane boundary conditions on elastic buckling behavior of solid and perforated plates, Thin-Walled Struct. 90 (2015) 171–181, http://dx.doi.org/10.1016/j.tws.2014.12.015.

[28] K. Liew, J. Wang, M. Tan, S. Rajendran, Postbuckling analysis of laminated composite plates using the mesh-free kp-Ritz method, Comput. Methods Appl. Mech. Engrg. 195 (7–8) (2006) 551–570, http://dx.doi.org/10.1016/j.cma.2005.02.004.

[29] S.K. Panda, L.S. Ramachandra, Buckling and postbuckling behavior of cross-ply composite plate subjected to nonuniform in-plane loads, J. Eng. Mech. 137 (9) (2011) 589–597, http://dx.doi.org/10.1061/(asce)em.1943-7889.0000258.

[30] P. Dash, B. Singh, Buckling and post-buckling of laminated composite plates, Mech. Res. Commun. 46 (2012) 1–7, http://dx.doi.org/10.1016/j.mechrescom.2012.08.002.

[31] A. Upadhyay, K. Shukla, Post-buckling behavior of composite and sandwich skew plates, Int. J. Non-Linear Mech. 55 (2013) 120–127, http://dx.doi.org/10.1016/j.ijnonlinmec.2013.05.010.

[32] D. Wang, J. Hui, W. Cao, Y. Yang, Y. Wan, H. Zuo, B. Zhang, The influence of geometric imperfections on post-buckling behavior and free vibrations of a fiber-reinforced composite laminated plate under thermal loading, Compos. Struct. 306 (2023) 116568, http://dx.doi.org/10.1016/j.compstruct.2022.116568.

[33] A. Bhimaraddi, Buckling and post-buckling behavior of laminated plates using the generalized nonlinear formulation, Int. J. Mech. Sci. 34 (9) (1992) 703–715, http://dx.doi.org/10.1016/0020-7403(92)90003-y.

[34] B. Wu, A. Pagani, M. Filippi, W. Chen, E. Carrera, Large-deflection and post-buckling analyses of isotropic rectangular plates by Carrera Unified Formulation, Int. J. Non-Linear Mech. 116 (2019) 18–31, http://dx.doi.org/10.1016/j.ijnonlinmec.2019.05.004.

[35] A. Pagani, E. Daneshkhah, X. Xu, E. Carrera, Evaluation of geometrically nonlinear terms in the large-deflection and post-buckling analysis of isotropic rectangular plates, Int. J. Non-Linear Mech. 121 (2020) 103461, http://dx.doi.org/10.1016/j.ijnonlinmec.2020.103461.

[36] E. Carrera, R. Azzara, E. Daneshkhah, A. Pagani, B. Wu, Buckling and post-buckling of anisotropic flat panels subjected to axial and shear in-plane loadings accounting for classical and refined structural and nonlinear theories, Int. J. Non-Linear Mech. 133 (2021) 103716, http://dx.doi.org/10.1016/j.ijnonlinmec.2021.103716.

[37] J.S.C. Praciano, P.S.B. Barros, E.S. Barroso, E. Parente, Á.S. de Holanda, J.B.M. Sousa, An isogeometric formulation for stability analysis of laminated plates and shallow shells, Thin-Walled Struct. 143 (2019) 106224, http://dx.doi.org/10.1016/j.tws.2019.106224.

[38] Y. Zhou, I. Stanciulescu, T. Eason, M. Spottswood, Nonlinear elastic buckling and postbuckling analysis of cylindrical panels, Finite Elem. Anal. Des. 96 (2015) 41–50, http://dx.doi.org/10.1016/j.finel.2014.12.001.

[39] X. Chen, Y. Lu, Z. Wu, Y. Shao, X. Xue, Y. Wu, Free vibration of in-plane bi-directional functionally graded materials rectangular plates with geometric imperfections and general elastic restraints, Aerosp. Sci. Technol. 132 (2023) 108045, http://dx.doi.org/10.1016/j.ast.2022.108045.

[40] H. Fukunaga, N. Hu, G. Ren, FEM modeling of adaptive composite structures using a reduced higher-order plate theory via penalty functions, Int. J. Solids Struct. 38 (48–49) (2001) 8735–8752, http://dx.doi.org/10.1016/s0020-7683(01)00072-5.

[41] B.R. Thakur, S. Verma, B. Singh, D. Maiti, Geometrically nonlinear dynamic analysis of laminated composite plate using a nonpolynomial shear deformation theory, Int. J. Non-Linear Mech. 128 (2021) 103635, http://dx.doi.org/10.1016/j.ijnonlinmec.2020.103635.

[42] J.N. Reddy, An Introduction to Nonlinear Finite Element Analysis, second ed., Oxford University Press, 2014, http://dx.doi.org/10.1093/acprof:oso/9780199641758.001.0001.

[43] V. Barathan, V. Rajamohan, M. Haboussi, G. Manickam, Variable stiffness composite laminated beams - nonlinear free flexural vibration behavior using a sinusoidal based shear flexible structural theory accounting for Poisson's effect, Int. J. Non-Linear Mech. 146 (2022) 104146, http://dx.doi.org/10.1016/j.ijnonlinmec.2022.104146.

[44] N. Grover, D. Maiti, B. Singh, A new inverse hyperbolic shear deformation theory for static and buckling analysis of laminated composite and sandwich plates, Compos. Struct. 95 (2013) 667–675, http://dx.doi.org/10.1016/j.compstruct.2012.08.012.

[45] Y. Joshan, N. Grover, B. Singh, A new non-polynomial four variable shear deformation theory in axiomatic formulation for hygro-thermo-mechanical analysis of laminated composite plates, Compos. Struct. 182 (2017) 685–693, http://dx.doi.org/10.1016/j.compstruct.2017.09.029.

[46] M.K. Prabhakara, Post-buckling behaviour of simply-supported cross-ply rectangular plates, Aeronaut. Q. 27 (4) (1976) 309–316, http://dx.doi.org/10.1017/s0001925900007812.

[47] J. Giri, G. Simitses, Deflection response of general laminated composite plates to in-plane and transverse loads, Fibre Sci. Technol. 13 (3) (1980) 225–242, http://dx.doi.org/10.1016/0015-0568(80)90006-8.

[48] S.K. Panda, L. Ramachandra, Buckling of rectangular plates with various boundary conditions loaded by non-uniform inplane loads, Int. J. Mech. Sci. 52 (6) (2010) 819–828, http://dx.doi.org/10.1016/j.ijmecsci.2010.01.009.

[49] M. Ganapathi, O. Polit, M. Touratier, A C0 eight-node membrane-shear-bending element for geometrically non-linear (static and dynamic) analysis of laminates, Internat. J. Numer. Methods Engrg. 39 (20) (1996) 3453–3474, http://dx.doi.org/10.1002/(sici)1097-0207(19961030)39:20<3453::aid-nme9>3.0.co;2-7.